Rotational bands in ^{170}Yb and ^{171}Yb and the projected shell model

D. E. Archer
Department of Physics, Florida State University, Tallahassee, Florida 32306
and Lawrence Livermore National Laboratory, Livermore, California 94550

M. A. Riley, T. B. Brown, D. J. Hartley, J. Döring, G. D. Johns, J. Pfohl, and S. L. Tabor
Department of Physics, Florida State University, Tallahassee, Florida 32306

J. Simpson
CCLRC Daresbury Laboratory, Daresbury Warrington, WA4 4AD, United Kingdom

Y. Sun
Joint Institute for Heavy Ion Research, ORNL, Oak Ridge, Tennessee 37831
and Department of Physics and Atmospheric Science, Drexel University, Philadelphia, Pennsylvania 19104

J. L. Egido
Departamento de Física Teórica C-XI, Universidad Autónoma de Madrid, E-28049 Madrid, Spain
(Received 14 August 1997)

Rotational bands in ^{170}Yb and ^{171}Yb have been studied with the reactions ^{170}Er$(\alpha,xn)^{174-x}$Yb at 35 and 40 MeV. Considerable extensions have been made to the previously published level schemes, and new structures have been found in each nucleus. Angular correlation measurements and reduced transition probability $[B(M1{:}I\rightarrow I-1)/B(E2{:}I\rightarrow I-2)]$ ratios have been extracted. Detailed comparisons are made with the first major projected shell model calculations for excited bands in an odd-N nucleus ^{171}Yb.
[S0556-2813(98)04206-X]

PACS number(s): 21.10.Re, 21.60.Cs, 23.20.Lv, 27.70.+q

I. INTRODUCTION

In high-spin spectroscopy studies of rare-earth nuclei, the isotopes of ytterbium ($Z=70$) have been a central focus for many experiments, and a large body of data has been established from $A=156$ to 168 [1], making it probably the best studied isotopic chain in the $A\approx160$ region. However, it is not possible to use the standard (HI,xn) fusion evaporation reactions to populate Yb nuclei beyond $A=168$. For the heavier $A=174$ to 178 nuclei [2], recent work using deep inelastic reactions and Gammasphere have begun to reveal much information about the high-spin behavior of these neutron-rich Yb isotopes. In the present work we have used the available α beam at Florida State University, together with the Pitt-FSU escape-suppressed Ge array [3] to perform detailed high-spin measurements on ^{170,171}Yb. Considerable extensions have been made to the level schemes of these nuclei and new structures have been observed.

The projected shell model (PSM) [4] has emerged as a very powerful method for describing high-spin level spectra. Several theoretical studies using this model have been performed for the yrast states in the well deformed rare-earth region [5–7]. Studies have also been successfully extended to excited bands, for example, for the even-even ^{168}Yb [8], and for several odd-Z Ta isotopes [9–11]. Currently, no major calculations have been performed for excited bands of an odd-N nucleus. In this work the model predictions are compared with the new experimental results for ^{171}Yb.

II. EXPERIMENTAL METHODS AND RESULTS

High-spin states of ^{170}Yb and ^{171}Yb were produced using the reaction ^{170}Er$(\alpha,xn)^{174-x}$Yb at beam energies of 35 and 40 MeV. The beam was provided by the FN Tandem and the Superconducting Linear Accelerators at Florida State University. Two stacked self-supporting ^{170}Er foils of thickness 1 mg/cm^2 were used as targets. The de-excitation γ rays were detected in the Pittsburgh-Florida State Universities γ array, consisting of 10 escape-suppressed Ge detectors and a 28 element BGO multiplicity filter [3]. At 40 MeV, a total of 33×10^6 prompt γ-γ events were collected when two or more suppressed Ge detectors were in coincidence and, at 35 MeV, 18×10^6 events were collected.

The spectra from the Ge detectors were gain matched off line, and a 4000×4000 matrix was created for each experiment using all possible combinations of coincidence pairs. The γ-ray energy and detection efficiency were calibrated using ^{152}Eu and ^{133}Ba sources. The low-energy portion of the efficiency curve was supplemented by coincidence data from the even-even ^{170}Yb data. The γ-ray data was then analyzed using the program ESCL8R created by Radford [12]. In addition, an angular correlation matrix was created for each nucleus by projecting the events from the 6 Ge detectors at 35° and 145° onto the x axis and the events from 4 Ge detectors at 90° onto the y axis. Analysis of the latter provides directional correlation (DCO) information which was used to assign multipolarities to γ-ray transitions of interest.

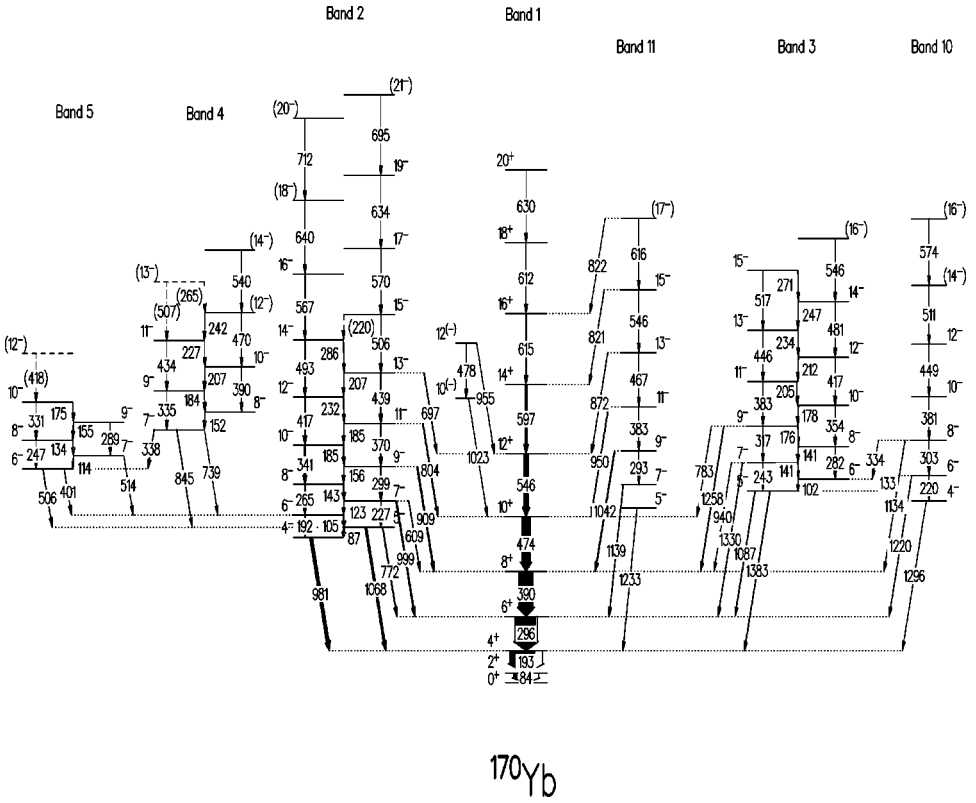

FIG. 1. Level scheme for negative parity bands in ^{170}Yb plotted with the positive parity ground-state band.

A. Results for ^{170}Yb

The present study has confirmed and extended the previously published level scheme by Walker *et al.* [13], who also used the (α,xn) reaction. In the present study, 67 new γ rays and 2 new band structures have been added to the level scheme shown in Figs. 1 and 2. Table I contains information on ^{170}Yb including γ ray energies, relative intensities, branching ratios (λ), DCO ratios, initial and final spin assignments. The spins have been assigned (or confirmed) using the present DCO ratios along with previously published data. A plot of the DCO ratios as a function of transition energy is given in Fig. 3. In this figure, as expected, the stretched $E2$ transitions are grouped around a DCO ratio of ≈ 1.0 and stretched dipoles around a DCO of ≈ 0.5.

Band 1, the positive parity yrast band. Previous work [13] observed this $K^{\pi}=0^{+}$ band tentatively to $I^{\pi}=20^{+}$. The present study confirms this tentative assignment. This band is shown in Fig. 4 panel (a), where a spectrum in coincidence with the 615 keV $16^{+}\rightarrow 14^{+}$ transition is presented.

Band 2, the lowest-energy negative parity band. Previous work [13] observed this band to a tentative maximum angular momentum of $17\hbar$ at an excitation energy of 3.7 MeV.

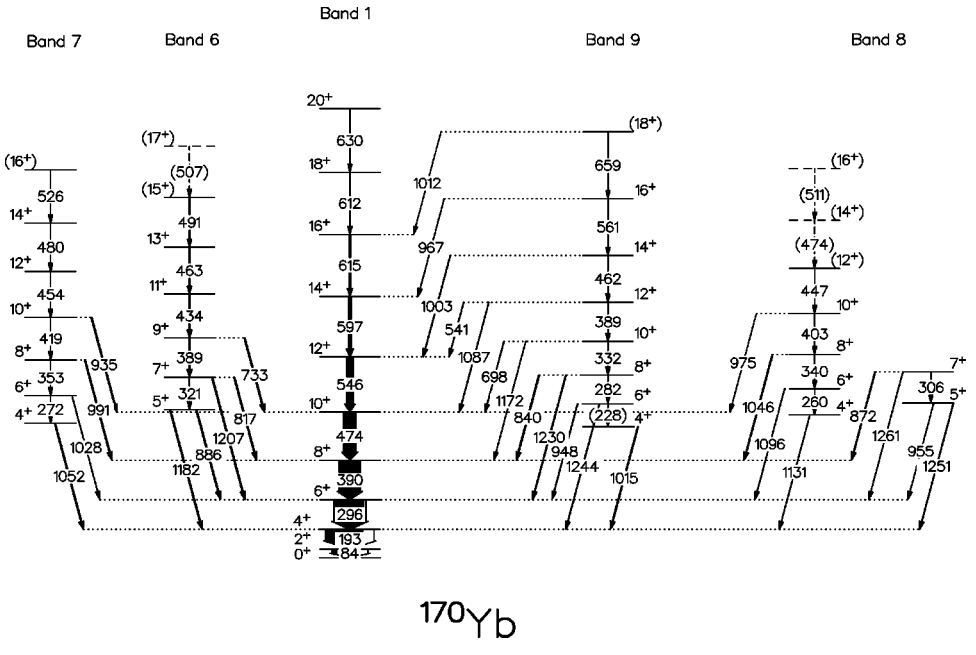

FIG. 2. Level scheme for positive parity bands in ^{170}Yb.

TABLE I. Data for ^{170}Yb.

E_x (keV) [a]	E_γ (keV) [b]	I_γ^{rel} [c]	λ [d]	DCO	I_i^π [e]	I_f^π [e]
			Band 1, $\alpha=0$			
84.4	84.4				2^+	0^+
277.6	193.2	364±10		1.03±0.01	4^+	2^+
573.3	295.7	300			6^+	4^+
963.2	389.9	205±6		1.06±0.01	8^+	6^+
1437.4	474.2	120±4		1.04±0.01	10^+	8^+
1983.1	545.7	65±2		1.04±0.01	12^+	10^+
2580.1	597.0	33±1		1.01±0.01	14^+	12^+
3194.9	614.8	11.2±0.8		1.07±0.03	16^+	14^+
3806.6	611.7	3.4±0.4		1.03±0.04	18^+	16^+
4436.3	629.7	0.4±0.2		1.2±0.4	20^+	18^+
			Band 2, $\alpha=0$			
1258.6	981.0	39±2		1.12±0.03	4^-	4^+
1450.5	191.9	5.3±0.3	1.1±0.1	1.02±0.08	6^-	4^-
	105.2	4.7±0.3		0.37±0.01	6^-	5^-
1715.9	265.4	11.2±0.1	2.4±0.1	1.16±0.04	8^-	6^-
	143.2	4.7±0.3		0.35±0.01	8^-	7^-
2056.7	340.8	16.9±0.3	5.7±0.6	1.07±0.03	10^-	8^-
	184.6	3.0±0.3		0.31±0.02	10^-	9^-
2473.7	417.0	14.5±0.3	7.7±1.2	0.99±0.02	12^-	10^-
	231.6	1.9±0.3			12^-	11^-
2966.4	492.7	7.9±0.3	7±1	0.96±0.03	14^-	12^-
	285.7	1.2±0.2			14^-	13^-
3533.8	567.4	4.3±0.3		0.96±0.04	16^-	14^-
4174.0	640.2	0.8±0.1			(18^-)	16^-
4885.9	711.9	0.3±0.1			(20^-)	(18^-)
			Band 2, $\alpha=1$			
1345.3	86.8	2.0±0.2		0.50±0.03	5^-	4^-
	771.8	8.3±0.4		0.78±0.06	5^-	6^+
	1067.7	25±1		0.64±0.03	5^-	4^+
1572.9	227.5	2.9±0.2		1.09±0.09	7^-	5^-
	122.6	0.9±0.2	3.4±0.9	0.72±0.05	7^-	6^-
	609.2	4.7±0.3		0.69±0.04	7^-	8^+
	999.3	13.8±0.6		0.58±0.02	7^-	6^+
1872.1	299.2	8.7±0.3		1.05±0.04	9^-	7^-
	156.4	1.7±0.2	5.2±0.5	0.37±0.03	9^-	8^-
	908.8	14.5±0.5		0.59±0.02	9^-	8^+
2242.0	369.9	10.3±0.3		1.03±0.05	11^-	9^-
	185.3	1.1±0.1	9±1	0.39±0.04	11^-	10^-
	804.3	9.7±0.3		0.53±0.02	11^-	10^+
2680.6	438.7	10.7±0.3		1.02±0.04	13^-	11^-
	206.9	0.5±0.2			13^-	12^-
	697.5	5.3±0.2		0.64±0.04	13^-	12^+
3186.3	505.7	7.1±0.3		0.99±0.08	15^-	13^-
	(220) [f]	<0.3			15^-	14^-
3756.6	570.3	4.6±0.2		1.04±0.07	17^-	15^-
4390.4	633.8	0.4±0.1		1.3±0.2	19^-	17^-
5084.9	694.5	0.4±0.1			(21^-)	19^-
			Band 3, $\alpha=1$			
1660.3	1086.8	5.2±0.5			5^-	6^+
	1382.9	5.2±0.6		0.8±0.1	5^-	4^+
1903.1	243.2	1.0±0.3		1.1±0.1	7^-	5^-
	141.0	0.2±0.1			7^-	6^-
	939.6	2.0±0.3		0.60±0.09	7^-	8^+
	1329.8	4.1±0.5		0.62±0.05	7^-	6^+

TABLE I. (*Continued*).

E_x (keV) [a]	E_γ (keV) [b]	I_γ^{rel} [c]	λ [d]	DCO	I_i^π [e]	I_f^π [e]
2220.6	317.5	1.5±0.2		1.0±0.1	9^-	7^-
	175.9	1.4±0.2			9^-	8^-
	783.1	1.5±0.2		0.72±0.08	9^-	10^+
	1257.6	6.0±0.4		0.45±0.08	9^-	8^+
2603.5	382.9	3.7±0.2		1.0±0.3	11^-	9^-
	205.1	1.7±0.1		0.62±0.04	11^-	10^-
3049.9	446.4	2.2±0.2		1.0±0.1	13^-	11^-
	234.3	1.0±0.1			13^-	12^-
3567.3	517.4	1.1±0.2		1.0±0.3	15^-	13^-
	270.8	0.4±0.1			15^-	14^-
			Band 3, $\alpha=0$			
1762.7	102.4	0.3±0.1			6^-	5^-
2044.6	281.9	2.4±0.3	1.2±0.2	1.2±0.2	8^-	6^-
	141.5	2.1±0.2			8^-	7^-
2398.5	353.9	3.9±0.2	1.5±0.1	1.02±0.09	10^-	8^-
	177.8	2.6±0.2			10^-	9^-
2815.7	417.2	3.2±0.2	2.2±0.3	0.93±0.08	12^-	10^-
	212.1	1.5±0.1		0.56±0.07	12^-	11^-
3296.5	480.7	2.2±0.2	4.0±0.9		14^-	12^-
	246.7	0.5±0.1			14^-	13^-
3842.3	545.8	0.6±0.2			(16^-)	14^-
			Band 4, $\alpha=1$			
2189.7	338.3	3.1±0.2			7^-	6^-
	739.2	0.4±0.2			7^-	6^-
	844.6	3.4±0.3		1.1±0.1	7^-	5^-
2525.2	335.4	0.4±0.2	0.15±0.06	1.3±0.2	9^-	7^-
	183.6	2.6±0.2			9^-	8^-
2959.6	434.4	2.3±0.3	1.7±0.3	0.9±0.1	11^-	9^-
	227.0	1.3±0.1			11^-	10^-
3466	(507) [f]	1.0±0.2			(13^-)	11^-
	(265) [f]	0.5±0.2			(13^-)	12^-
			Band 4, $\alpha=0$			
2341.7	152.0	2.4±0.2			8^-	7^-
2732.4	390.5	1.3±0.2	0.4±0.1		10^-	8^-
	207.3	3.1±0.3			10^-	9^-
3202.2	469.9	0.9±0.2	0.6±0.1		(12^-)	10^-
	242.5	1.5±0.2			(12^-)	11^-
3742.2	540.0	0.4±0.1			(14^-)	(12^-)
			Band 5, $\alpha=0$			
1851.4	400.9	1.9±0.2			6^-	6^-
	505.9	4.1±0.4			6^-	5^-
2098.7	247.0	0.5±0.2			8^-	6^-
	133.9	1.7±0.2			8^-	7^-
2429.2	330.7	1.5±0.2			10^-	8^-
	175.4	1.4±0.2			10^-	9^-
2847.3	(418) [f]	1.4±0.3			(12^-)	10^-
			Band 5, $\alpha=1$			
1964.9	113.6	0.6±0.2			7^-	6^-
	514.3	1.2±0.2			7^-	6^-
2253.7	288.8	1.1±0.3			9^-	7^-
	154.9	1.5±0.2			9^-	8^-
			Band 6, $\alpha=1$			
1459.7	886.5	1.4±0.5		0.8±0.2	5^+	6^+
	1182.2	4.0±0.7		0.69±0.07	5^+	4^+

TABLE I. (*Continued*).

E_x (keV) [a]	E_γ (keV) [b]	I_γ^{rel} [c]	λ [d]	DCO	I_i^π [e]	I_f^π [e]
1780.3	320.6	0.8±0.3			7^+	5^+
	817.1	2.9±0.4		0.48±0.05	7^+	8^+
	1207.0	16±2		0.51±0.02	7^+	6^+
2169.4	389.1	11±2			9^+	7^+
	732.9	0.8±0.2			9^+	10^+
2603.2	433.8	6.7±0.7		0.86±0.04	11^+	9^+
3066.4	463.2	2.9±0.4		1.14±0.09	13^+	11^+
3557.5	491.1	1.4±0.2			(15^+)	13^+
4064.3	(507) [f]	0.6±0.2			(17^+)	(15^+)
			Band 7, $\alpha=0$			
1329.6	1051.8	5.5±0.9			4^+	4^+
1601.4	271.6	0.2±0.1			6^+	4^+
	1028.1	2.8±0.6		0.51±0.02	6^+	6^+
1954.1	352.8	1.2±0.3		1.00±0.01	8^+	6^+
	990.8	4.4±0.5		0.6±0.1	8^+	8^+
2372.7	418.7	1.2±0.2		1.0±0.1	10^+	8^+
	935.3	1.3±0.3		0.9±0.3	10^+	10^+
2826.7	454.0	1.8±0.2		1.1±0.2	12^+	10^+
3307.2	480.5	1.1±0.2		1.1±0.2	14^+	12^+
3833.2	526.0	0.8±0.2			(16^+)	14^+
			Band 8, $\alpha=0$			
1408.9	1131.3	2.5±0.8		1.1±0.2	4^+	4^+
1669.0	260.4	0.4±0.2			6^+	4^+
	1095.8	2.7±0.5		0.70±0.06	6^+	6^+
2009.3	340.4	1.6±0.3			8^+	6^+
	1046.0	8.1±0.9		0.97±0.07	8^+	8^+
2412.3	403.1	1.6±0.3		1.1±0.2	10^+	8^+
	974.8	0.9±0.2		0.9±0.1	10^+	10^+
2859.1	446.8	1.2±0.2			(12^+)	10^+
3333.3	(474) [f]	1.0±0.5			(14^+)	(12^+)
2859.1	(511) [f]	0.6±0.3			(16^+)	(14^+)
			Band 8, $\alpha=1$			
1528.9	955.2	1.5±0.6		0.92±0.09	5^+	6^+
	1251.3	4.3±0.9		0.7±0.1	5^+	4^+
1835.0	306.1	0.7±0.4			7^+	5^+
	871.8	7.2±0.8		0.55±0.03	7^+	8^+
	1261 [f]	2.2±0.5		0.67±0.08	7^+	6^+
			Band 9, $\alpha=0$			
1292.4	1014.7	9±2		1.2±0.2	4^+	4^+
1521.2	(228.2)	0.5±0.2			6^+	4^+
	948.0	4.4±0.6			6^+	6^+
	1243.6	4.6±0.9		1.1±0.3	6^+	4^+
1803.4	281.8	1.8±0.5			8^+	6^+
	840.1	10±1		1.0±0.1	8^+	8^+
	1230.3	6.3±0.9		1.3±0.1	8^+	6^+
2135.2	331.9	1.5±0.4		0.9±0.1	10^+	8^+
	697.8	3.4±0.6		0.84±0.04	10^+	10^+
	1172.3	1.8±0.5		1.0±0.2	10^+	8^+
2523.9	389.2	1.8±0.2		0.88±0.04	12^+	10^+
	540.6	2.9±0.5		0.88±0.04	12^+	12^+
	1086.8	3.2±0.5		1.1±0.1	12^+	10^+
2986.3	462.4	1.8±0.3		0.9±0.1	14^+	12^+
	1003.3	4.2±0.5			14^+	12^+

TABLE I. (*Continued*).

E_x (keV) [a]	E_γ (keV) [b]	I_γ^{rel} [c]	λ [d]	DCO	I_i^π [e]	I_f^π [e]
3546.9	560.6	0.9±0.5			16^+	14^+
	966.9	1.6±0.2		0.8±0.1	16^+	14^+
4206.3	659.4	0.3±0.2			(18^+)	16^+
	1012.4	0.6±0.2			(18^+)	16^+
			Band 10, $\alpha=0$			
1573.3	1295.7	4.0±0.6			4^-	4^+
1793.8	220.5	0.8±0.3		0.9±0.1	6^-	4^-
	132.9	0.7±0.2			6^-	5^-
	1220.2	3±1		1.2±0.3	6^-	6^+
2097.1	303.3	3.2±0.6		1.11±0.06	8^-	6^-
	334.4	<0.5			8^-	6^-
	1133.6	2.2±0.3			8^-	8^+
2478.1	381.0	1.5±0.3		1.03±0.09	10^-	8^-
2927.5	449.4	1.0±0.2		1.0±0.2	12^-	10^-
3438.1	510.6	0.8±0.3			(14^-)	12^-
4013.7	574 [f]	<0.5			(16^-)	(14^-)
			Band 11, $\alpha=1$			
1510.4	1232.8	1.6±0.7		0.7±0.1	5^-	4^+
1712.4	1139.1	4.0±0.6		0.59±0.07	7^-	6^+
2005.3	292.9	0.6±0.2			9^-	7^-
	1042.1	10.3±0.9		0.61±0.04	9^-	8^+
2387.9	382.6	0.8±0.2			11^-	9^-
	950.5	6.3±0.6		0.55±0.03	11^-	10^+
2855.4	467.5	0.9±0.2		1.0±0.1	13^-	11^-
	872.3	2.1±0.3		0.55±0.03	13^-	12^+
3401.5	546.1	1.0±0.5			15^-	13^-
	821.4	1.9±0.3		0.6±0.1	15^-	14^+
4017.5	616.0	0.6±0.3			(17^-)	15^-
	822 [f]	<0.3			(17^-)	16^+
			Other transitions			
2460.4	1023.0	0.8±0.2		1.0±0.2	$10^{(-)}$	10^+
2938.4	478.0	0.9±0.1		1.1±0.4	$12^{(-)}$	$10^{(-)}$
	955.3	0.5±0.2		1.1±0.2	$12^{(-)}$	12^+

[a]Level energies; bandhead excitation energies have been taken from previous work [13].

[b]γ-ray energies taken from 40 MeV data set. Accurate to 0.2 keV for most transitions. For weak or contaminated transitions, accurate to 0.5 keV.

[c]Relative γ-ray intensities [$I_\gamma(295.7)\equiv 300$] measured in the 40 MeV data set.

[d]Branching ratio $\lambda = I_\gamma(I\rightarrow I-2)/I_\gamma(I\rightarrow I-1)$ measured from spectra corresponding to gates above spin I.

[e]Spin and parity assignments are based on the previous work [13] and on the assumption that the character of the new transitions within bands continues being stretched $E2$ in nature.

[f]Accurate to within 1 keV.

The present study extends this band to $(21)\hbar$ at an excitation energy of 5.08 MeV. A spectrum of this band can be seen in Fig. 4 panel (b). Walker *et al.* [13] identified the bandhead to be $K=4$ with a lifetime of 370±15 ns.

Band 3. This strongly coupled band has only 20% of the intensity of band 2. The present study has extended the $\alpha=1$ signature by $2\hbar$ and the $\alpha=0$ signature by $4\hbar$ over the previous work [13]. The $\alpha=1$ signature feeds strongly to the positive parity yrast band, by dipole radiation to the 10^+ level and below.

Bands 4 and 5. This study confirms the assignment of spins and transition energies made to these two bands by Walker *et al.* [13]. In addition, in-band stretched $E2$ transitions in the $\alpha=0$ signature of band 4 have been identified for the first time in this study, as well as one transition in the $\alpha=1$ signature of band 5. A sample spectrum for band 4 is shown in Fig. 4(c).

Bands 6 and 7. These two bands are based upon the 1146 keV 2^+ state and have been identified by Riedinger *et al.* [14], through Coulomb excitation as γ-vibrational bands. Additions to these bands were made by Walker *et al.* [13]. In the present study, a 389 keV γ ray has been added to band 6 at the 9^+ level, moving the 434 keV γ ray to the 11^+ level, and building the sequence to a tentative 17^+ level. Although the 389 keV transition is a very strong γ-ray transition in the yrast band, the 733 keV $9^+\rightarrow 10^+$ transition establishes the energy of the 9^+ level in band 6.

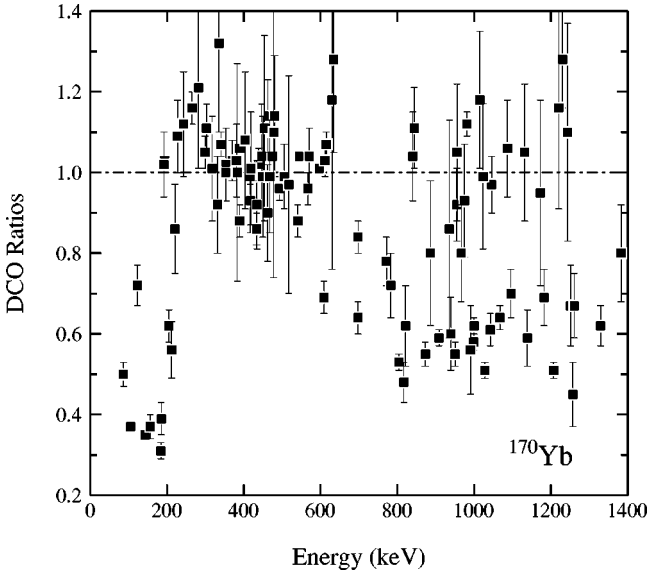

FIG. 3. DCO ratios as a function of γ-ray energy for transitions in ^{170}Yb.

Band 8. In the previous study [13], only two in-band transitions were observed, but feeding to the yrast band made it possible to determine the parity of the band. The previously known transitions have been confirmed, and both new transitions and new states have been added to this band extending it from spin $10\hbar$ to a tentative spin of $16\hbar$.

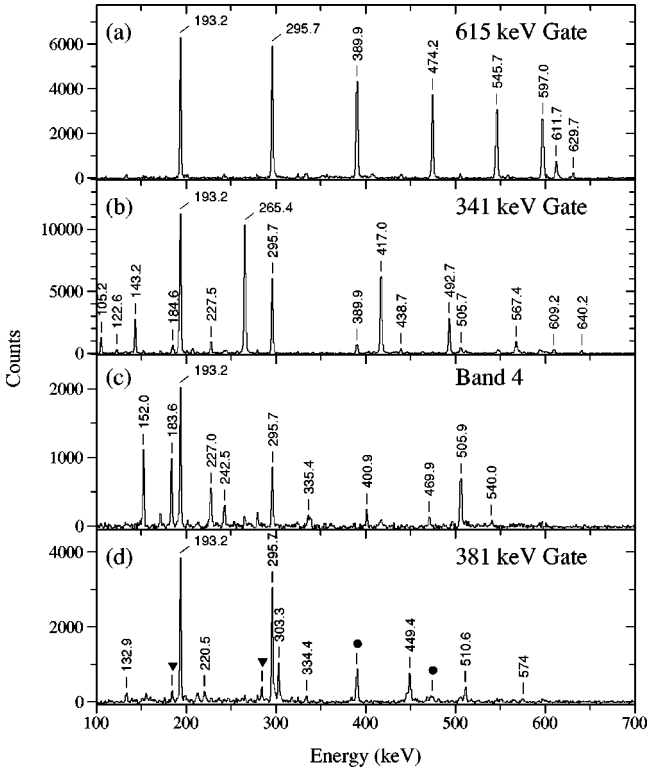

FIG. 4. Spectra for selected bands of ^{170}Yb. (a) Band 1: transitions in coincidence with the 615 keV transition. (b) Band 2: a gate on the 341 keV transition. (c) Band 4: a mathematical AND between gates on the 207 and 338 keV γ rays. (d) shows the new band (band 10) with a gate on the 381 keV transition. In panel (d), transitions marked by a filled $\triangledown$ are in an unplaced band of γ rays coincident with the 381 keV gate and the filled $\bigcirc$ denotes ground-state band γ rays.

Band 9. Band 9 decays predominantly to the positive parity yrast band, see Fig. 2 and Table I. The in-band stretched $E2$ γ rays have been identified for the first time, and the band has been extended from the tentative $I^{\pi}=(12)^{+}$ level to an $I^{\pi}=(18^{+})$ level.

Band 10. This new band consists of six stretched $E2$ transitions and feeds the positive parity yrast band at the 4^{+},6^{+}, and 8^{+} levels and the negative parity band 3 at the 5^{-} and 6^{-} levels. Spins were assigned to this band by the DCO measurements. Negative parity has been assigned based upon the 334 keV $\Delta I=2$ transition from band 10 to the 6^{-} state in band 3. A sample spectrum for this band can be seen in panel (d) of Fig. 4.

Band 11. Eight levels in this band were reported [13] (with the states of spins 1 and 3 being tentative), and no in-band γ ray was included apart from a tentative $15\hbar\rightarrow 13\hbar$ transition. In addition, parities of the spin $9\hbar$ and $11\hbar$ states were interpreted as negative and the band was assigned $K=(1)$ [13]. The present study adds four in-band γ rays, as well as three other new γ rays which feed the yrast band from the three highest levels in band 11. Parities of the states in this band were assigned based on the previous parity assignments [13] and the stretched $E2$ nature of the in-band γ rays.

Other transitions. Three transitions establishing two new levels at excitation energies of 2.460 and 2.938 MeV in ^{170}Yb have been found. These levels have not been identified with any other band in this nucleus, but they feed the positive parity yrast band at the 10^{+} and 12^{+} levels via transitions of energies 1023 and 955 keV, see Fig. 1.

B. Results for ^{171}Yb

The nucleus ^{171}Yb has been studied extensively by radioactive decay of ^{171}Lu [15–17] and by (d,t) and (d,p) reactions [18] making the low-energy levels of this nucleus well known. The reaction ^{170}Er$(\alpha,3n)$ at 26–34 MeV was used by Lindblad *et al.* [19] in a fusion evaporation experiment revealing high-spin states $(I\leqslant\frac{27}{2})$ built upon these well known low-lying states. This latter study has identified four rotational bands based upon the $[633]\frac{7}{2}^{+}$, $[521]\frac{1}{2}^{-}$, $[512]\frac{5}{2}^{-}$, and tentative $[505]\frac{11}{2}^{-}$ Nilsson states [19]. The present study has confirmed and extended the previously published level scheme identifying 110 new γ rays and 4 new bands. The level scheme formed in the present work is shown in Fig. 5. Three additional low-energy γ rays (<56 keV) not shown in our level scheme were established by Lindblad *et al.* [19] fixing the bandhead excitation energies of bands 1 and 3. Table II contains information from the present measurement on ^{171}Yb including γ-ray energies, relative intensities, branching ratios, DCO ratios, initial and final spins. The spins have been assigned (or confirmed) using the DCO ratios along with previously published information. A plot of the DCO ratios as a function of γ-ray energy is given in Fig. 6.

Band 1. Band 1 is the positive parity band based upon the $[633]\frac{7}{2}^{+}$ Nilsson state. A spectrum of this band is shown in Fig. 7(a). This band was previously identified to spin $\frac{27}{2}\hbar$

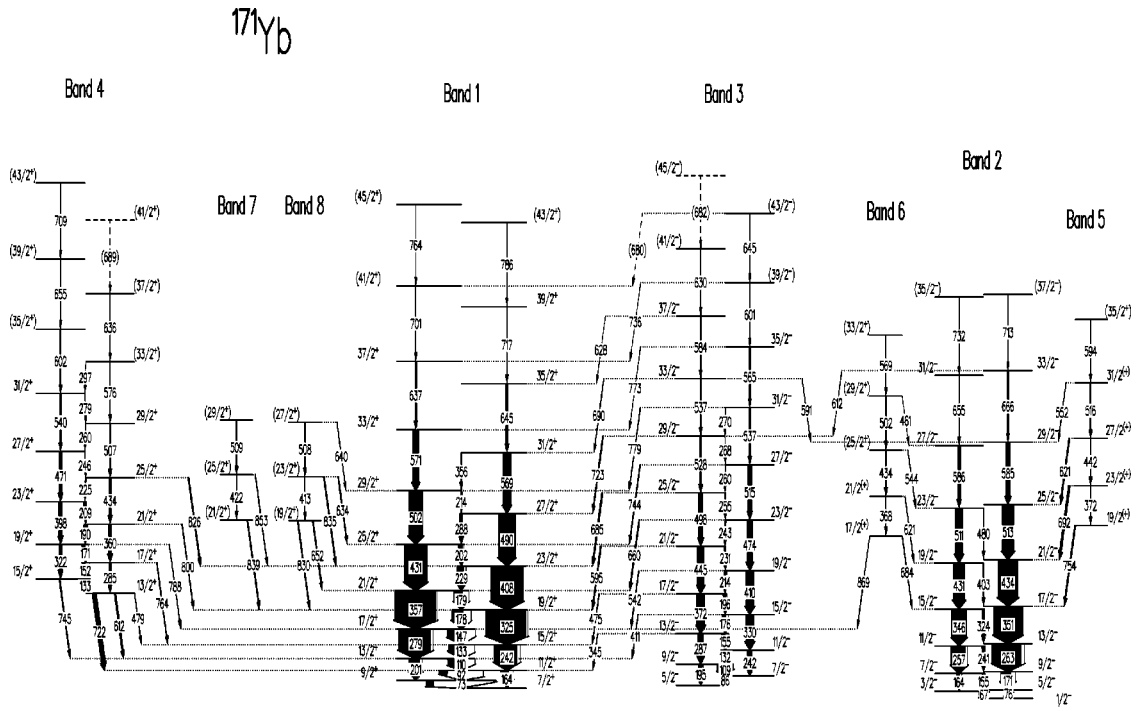

FIG. 5. Level scheme for ^{171}Yb.

[19] and has been extended to a spin of $(\frac{45}{2})\hbar$ in the present study.

Band 2. Band 2 is the band based upon the $[521]\frac{1}{2}^-$ Nilsson state. A spectrum of the favored signature in this band is shown in Fig. 7(b). The unfavored signature is shown by the spectrum in Fig. 7(c). This band was previously identified up to a tentative spin of $\frac{25}{2}\hbar$ [19]. The $\frac{25}{2}\rightarrow\frac{21}{2}$ transition has been confirmed, and the band has been extended to a spin of $(\frac{37}{2})\hbar$. This band exhibits large signature splitting. The $\frac{33}{2}$ state in band 2 comes within 70 keV of the $\frac{33}{2}$ state in band 3. These two states interact and cross transitions between the two bands are observed of energies 612 and 591 keV, see Fig. 5.

Band 3. This band is based upon the $[512]\frac{5}{2}^-$ Nilsson state. A spectrum of this band is shown in Fig. 7(d). Band 3 has been confirmed up to the previously known level of $\frac{21}{2}$ [19] and extended to a spin of $\frac{43}{2}\hbar$ and tentatively to $\frac{45}{2}\hbar$. Unlike the previous two bands discussed, this band shows no signature splitting, and it decays at every level between spins $I=\frac{13}{2}$ and $\frac{39}{2}$ by a $\Delta I=1$ transition to band 1.

Band 4. Previously this band was tentatively suggested as being based upon the $[505]\frac{11}{2}^-$ Nilsson state [19]. We, however, prefer an alternative assignment to this band. This is discussed further in Sec. V. A spectrum for this sequence is shown in Fig. 8(a). This band was previously identified up to the $\frac{21}{2}$ level [19]. The current study has extended this band to $(\frac{43}{2})\hbar$. Several new transitions linking this structure to band 1 have been identified.

Bands 5 and 6. Two new bands have been observed that feed band 2. These bands appear to be signature partners, as discussed below, but connecting $M1$ transitions were not observed. A structure similar to band 6 has been identified in ^{173}Hf [20], an isotone of ^{171}Yb. A transition linking band 6 directly to band 1 has been found. Sample spectra for bands 5 and 6 can be found in Fig. 8(b) and 8(c), respectively.

Bands 7 and 8. Two new very weakly populated ($I_\gamma \leqslant 3\%$ band 1) structures which decay to band 1 have been observed. The spin and parity assignments given are tentative.

III. PROJECTED SHELL MODEL

The projected shell model [4] (PSM) is a shell model approach starting from the deformed [21] single-particle basis. Its advantage over the conventional shell model is that the important nuclear correlations, especially for a strongly deformed system, are easily taken into account in a manageable configuration space, thus making it possible to treat the heavy systems within the shell model framework. We will not explain the details of the model here; the interested reader can learn the model from the review article [4]. Recently, the model has been used to give a possible explanation for the problem of the anomalous crossing frequency in the odd-proton rare-earth nuclei [22] and detailed comparisons were made with ^{168}Yb [8], ^{169}Ta [9], ^{177}Ta [10], and ^{175}Ta [11]. Thus the model space and the corresponding Hamiltonian used for this mass region are well justified.

The calculation starts with the ansatz for the angular momentum projected wave function given by

$$|IM\rangle=\sum_\kappa f_\kappa \hat{P}^I_{MK_\kappa}|\varphi_\kappa\rangle, \tag{1}$$

where κ labels the basis states. Acting on an intrinsic state $|\varphi_\kappa\rangle$, the operator $\hat{P}^I_{MK}$ [23] generates states of good angular momentum, thus restoring the necessary rotational symmetry violated in the deformed mean field. The basis states $|\varphi_\kappa\rangle$ are spanned by the set

$$\{\alpha^\dagger_{n_i}|\phi\rangle, \alpha^\dagger_{n_i}\alpha^\dagger_{n_j}\alpha^\dagger_{n_l}|\phi\rangle, \alpha^\dagger_{p_i}\alpha^\dagger_{p_j}\alpha^\dagger_{n_l}|\phi\rangle\} \tag{2}$$

TABLE II. Data for ^{171}Yb.

E_x (keV) [a]	E_γ (keV) [b]	I_γ^{rel} [c]	λ [d]	DCO	I_i^π [e]	I_f^π [e]
			Band 1, $\alpha = +\frac{1}{2}$			
168.0	72.8	89±3			$\frac{9}{2}+$	$\frac{7}{2}+$
369.3	201.4	128±7	1.4±0.1	1.04±0.04	$\frac{13}{2}+$	$\frac{9}{2}+$
	110.0	92±5		0.33±0.01	$\frac{13}{2}+$	$\frac{11}{2}+$
648.6	279.2	390±7	2.4±0.2	1.05±0.02	$\frac{17}{2}+$	$\frac{13}{2}+$
	147.0	160±13		0.39±0.01	$\frac{17}{2}+$	$\frac{15}{2}+$
1005.2	356.6	500	4.4±0.5	0.94±0.02	$\frac{21}{2}+$	$\frac{17}{2}+$
	178.8	114±11		0.37±0.01	$\frac{21}{2}+$	$\frac{19}{2}+$
1436.3	431.1	277±5	6.1±0.3	0.96±0.03	$\frac{25}{2}+$	$\frac{21}{2}+$
	201.7	45±2			$\frac{25}{2}+$	$\frac{23}{2}+$
1938.6	502.3	176±3	12±1	0.99±0.02	$\frac{29}{2}+$	$\frac{25}{2}+$
	213.8	14.3±0.9			$\frac{29}{2}+$	$\frac{27}{2}+$
2509.5	570.9	78±2		0.95±0.07	$\frac{33}{2}+$	$\frac{29}{2}+$
3147.0	637.5	19±1		1.0±0.1	$\frac{37}{2}+$	$\frac{33}{2}+$
3848.5	701.5	4.1±0.6			$(\frac{41}{2}+)$	$\frac{37}{2}+$
4612.6	764.1	<1			$(\frac{45}{2}+)$	$(\frac{41}{2}+)$
			Band 1, $\alpha = -\frac{1}{2}$			
259.3	164.1	97±10	1.0±0.1	1.20±0.06	$\frac{11}{2}+$	$\frac{7}{2}+$
	91.6	103±9		0.38±0.01	$\frac{11}{2}+$	$\frac{9}{2}+$
501.7	242.3	281±7	2.2±0.2	0.98±0.02	$\frac{15}{2}+$	$\frac{11}{2}+$
	132.7	127±12		0.41±0.01	$\frac{15}{2}+$	$\frac{13}{2}+$
826.5	324.8	488±6	3.5±0.4	1.03±0.02	$\frac{19}{2}+$	$\frac{15}{2}+$
	177.9	142±13		0.33±0.02	$\frac{19}{2}+$	$\frac{17}{2}+$
1234.7	408.2	390±5	4.7±0.1	0.97±0.02	$\frac{23}{2}+$	$\frac{19}{2}+$
	229.5	83.5±0.7		0.32±0.01	$\frac{23}{2}+$	$\frac{21}{2}+$
1724.9	490.2	205±4	6.8±0.4	0.95±0.03	$\frac{27}{2}+$	$\frac{23}{2}+$
	288.5	30±2		0.29±0.02	$\frac{27}{2}+$	$\frac{25}{2}+$
2294.3	569.4	92±3	9±2	0.99±0.09	$\frac{31}{2}+$	$\frac{27}{2}+$
	355.6	10±2			$\frac{31}{2}+$	$\frac{29}{2}+$
2939.5	645.2	25±2		0.99±0.06	$\frac{35}{2}+$	$\frac{31}{2}+$
3656.9	717.4	6.1±0.9		1.2±0.2	$\frac{39}{2}+$	$\frac{35}{2}+$
4442.9	786.0	<1			$(\frac{43}{2}+)$	$\frac{39}{2}+$
			Band 2, $\alpha = +\frac{1}{2}$			
76.1	76.1				$\frac{5}{2}-$	$\frac{1}{2}-$
247.1	171.0	127±13		1.16±0.02	$\frac{9}{2}-$	$\frac{5}{2}-$
509.8	262.7	362±7			$\frac{13}{2}-$	$\frac{9}{2}-$
860.5	350.7	341±5		1.04±0.02	$\frac{17}{2}-$	$\frac{13}{2}-$
1294.8	434.3	242±4		1.00±0.02	$\frac{21}{2}-$	$\frac{17}{2}-$
1807.8	513.0	139±3		1.05±0.03	$\frac{25}{2}-$	$\frac{21}{2}-$
2393.0	585.2	54±2		1.01±0.07	$\frac{29}{2}-$	$\frac{25}{2}-$
3059.0	666.0	11.4±0.9		0.9±0.3	$\frac{33}{2}-$	$\frac{29}{2}-$
	612.1	3±1			$\frac{33}{2}-$	$\frac{29}{2}-$
3772.5	713.5	2.3±0.6			$(\frac{37}{2}-)$	$\frac{33}{2}-$
			Band 2, $\alpha = -\frac{1}{2}$			
67.2	67.2				$\frac{3}{2}-$	$\frac{1}{2}-$
231.3	164.2	41±6	2.3±0.5	1.17±0.02	$\frac{7}{2}-$	$\frac{3}{2}-$
	155.1	17±2		1.05±0.02	$\frac{7}{2}-$	$\frac{5}{2}-$
488.0	256.7	180±5	5.8±0.4		$\frac{11}{2}-$	$\frac{7}{2}-$
	240.9	31±2		0.84±0.06	$\frac{11}{2}-$	$\frac{9}{2}-$
833.7	345.7	174±4	6.7±0.8	1.07±0.02	$\frac{15}{2}-$	$\frac{11}{2}-$
	323.9	26±3		0.74±0.02	$\frac{15}{2}-$	$\frac{13}{2}-$

TABLE II. (*Continued*).

E_x (keV) [a]	E_γ (keV) [b]	I_γ^{rel} [c]	λ [d]	DCO	I_i^π [e]	I_f^π [e]
1264.1	430.6	138±4	13±1	0.97±0.03	$\frac{19}{2}^-$	$\frac{15}{2}^-$
	403.4	10.9±0.9		0.87±0.06	$\frac{19}{2}^-$	$\frac{17}{2}^-$
1774.6	510.6	89±3	16±3	0.95±0.04	$\frac{23}{2}^-$	$\frac{19}{2}^-$
	479.7	5.6±0.9			$\frac{23}{2}^-$	$\frac{21}{2}^-$
2360.2	585.6	30±2		1.01±0.07	$\frac{27}{2}^-$	$\frac{23}{2}^-$
3015.5	655.3	8.3±0.3		1.2±0.2	$\frac{31}{2}^-$	$\frac{27}{2}^-$
3747.1	731.6	1.4±0.6			$(\frac{35}{2}^-)$	$\frac{31}{2}^-$
			Band 3, $\alpha = +\frac{1}{2}$			
317.6	195.2	52±7	1.0±0.2		$\frac{9}{2}^-$	$\frac{5}{2}^-$
	109.5	53±6		0.44±0.01	$\frac{9}{2}^-$	$\frac{7}{2}^-$
604.7	287.0	68±4		0.96±0.05	$\frac{13}{2}^-$	$\frac{9}{2}^-$
	154.9	45±5	1.5±0.2	0.46±0.02	$\frac{13}{2}^-$	$\frac{11}{2}^-$
	345.4	7±2		0.63±0.08	$\frac{13}{2}^-$	$\frac{11}{2}^+$
976.7	371.9	100±4		0.94±0.04	$\frac{17}{2}^-$	$\frac{13}{2}^-$
	196.1	30±3	3.3±0.4		$\frac{17}{2}^-$	$\frac{15}{2}^-$
	475.3	8±2			$\frac{17}{2}^-$	$\frac{15}{2}^+$
1421.8	445.0	80±3		1.07±0.08	$\frac{21}{2}^-$	$\frac{17}{2}^-$
	231.0	17±2	4.8±0.5	0.39±0.04	$\frac{21}{2}^-$	$\frac{19}{2}^-$
	595.5	14±2			$\frac{21}{2}^-$	$\frac{19}{2}^+$
1920.0	498.2	51±2		1.0±0.1	$\frac{25}{2}^-$	$\frac{21}{2}^-$
	254.8	8±1	6.1±0.8	0.4±0.1	$\frac{25}{2}^-$	$\frac{23}{2}^-$
	685.2	17±2		0.53±0.07	$\frac{25}{2}^-$	$\frac{23}{2}^+$
2446.9	527.7	24±2		0.9±0.1	$\frac{29}{2}^-$	$\frac{25}{2}^-$
	267.6	3.3±0.9	7±2		$\frac{29}{2}^-$	$\frac{27}{2}^-$
	722.8	13±2			$\frac{29}{2}^-$	$\frac{27}{2}^+$
2984.1	537.2	8±2		1.1±0.1	$\frac{33}{2}^-$	$\frac{29}{2}^-$
	690.2	6±1		0.6±0.1	$\frac{33}{2}^-$	$\frac{31}{2}^+$
	591.0	5.0±0.6		0.9±0.3	$\frac{33}{2}^-$	$\frac{29}{2}^-$
3567.9	583.8	6±1		1.1±0.2	$\frac{37}{2}^-$	$\frac{33}{2}^-$
	628.2	0.8±0.5			$\frac{37}{2}^-$	$\frac{35}{2}^+$
4198.4	630 [f]	<1			$(\frac{41}{2}^-)$	$\frac{37}{2}^-$
4880.5	(682) [f]	<1			$(\frac{45}{2}^-)$	$(\frac{41}{2}^-)$
			Band 3, $\alpha = -\frac{1}{2}$			
208.1	86.1				$\frac{7}{2}^-$	$\frac{5}{2}^-$
450.0	241.9	55±6	1.1±0.2		$\frac{11}{2}^-$	$\frac{7}{2}^-$
	132.5	48±4		0.42±0.01	$\frac{11}{2}^-$	$\frac{9}{2}^-$
780.6	330.5	96±4		1.06±0.04	$\frac{15}{2}^-$	$\frac{11}{2}^-$
	176.1	46±2	2.1±0.1	0.48±0.02	$\frac{15}{2}^-$	$\frac{13}{2}^-$
	411.4	8±2			$\frac{15}{2}^-$	$\frac{13}{2}^+$
1190.7	410.0	95±4		1.05±0.05	$\frac{19}{2}^-$	$\frac{15}{2}^-$
	214.1	25±2	3.8±0.3	0.42±0.02	$\frac{19}{2}^-$	$\frac{17}{2}^-$
	542.2	9±2		0.56±0.08	$\frac{19}{2}^-$	$\frac{17}{2}^+$
1665.2	474.4	70±3		1.07±0.07	$\frac{23}{2}^-$	$\frac{19}{2}^-$
	243.4	15±2	4.6±0.5		$\frac{23}{2}^-$	$\frac{21}{2}^-$
	660.1	14±2		0.7±0.3	$\frac{23}{2}^-$	$\frac{21}{2}^+$
2180.1	514.9	42±2		0.98±0.06	$\frac{27}{2}^-$	$\frac{23}{2}^-$
	260.1	4.8±0.9	9±2	0.7±0.1	$\frac{27}{2}^-$	$\frac{25}{2}^-$
	744.3	10±2			$\frac{27}{2}^-$	$\frac{25}{2}^+$
2717.3	537.2	20±2		1.1±0.4	$\frac{31}{2}^-$	$\frac{27}{2}^-$
	269.6	1.6±0.5	12±4		$\frac{31}{2}^-$	$\frac{29}{2}^-$
	779.3	7±1		0.6±0.1	$\frac{31}{2}^-$	$\frac{29}{2}^+$

TABLE II. (*Continued*).

E_x (keV) [a]	E_γ (keV) [b]	I_γ^{rel} [c]	λ [d]	DCO	I_i^π [e]	I_f^π [e]
3282.0	564.7	12±2		1.0±0.1	$\frac{35}{2}^-$	$\frac{31}{2}^-$
	773.0	2.3±0.6		0.6±0.1	$\frac{35}{2}^-$	$\frac{33}{2}^+$
3882.8	600.8	5.3±0.9			$(\frac{39}{2}^-)$	$\frac{35}{2}^-$
	736.3	0.9±0.3			$(\frac{39}{2}^-)$	$\frac{37}{2}^+$
4528.0	645 [f]	<0.5			$(\frac{43}{2}^-)$	$(\frac{39}{2}^-)$
	(680) [f]	<0.5			$(\frac{43}{2}^-)$	$(\frac{41}{2}^+)$
			Band 4, $\alpha = -\frac{1}{2}$			
1114.4	745.2	13±2			$\frac{15}{2}^+$	$\frac{13}{2}^+$
	133.2	57±6		0.48±0.02	$\frac{15}{2}^+$	$\frac{13}{2}^+$
1436.9	322.5	34±4		1.07±0.07	$\frac{19}{2}^+$	$\frac{15}{2}^+$
	171.0	49±5	0.7±0.1	0.33±0.02	$\frac{19}{2}^+$	$\frac{17}{2}^+$
	788.3	6±1			$\frac{19}{2}^+$	$\frac{17}{2}^+$
1835.1	398.1	41± 4	1.8±0.3	0.97±0.06	$\frac{23}{2}^+$	$\frac{19}{2}^+$
	208.7	22±2		0.26±0.02	$\frac{23}{2}^+$	$\frac{21}{2}^+$
2306.6	471.4	35±4	4.4±0.8	1.0±0.1	$\frac{27}{2}^+$	$\frac{23}{2}^+$
	246.5	8±1		0.44±0.06	$\frac{27}{2}^+$	$\frac{25}{2}^+$
2846.7	540.1	17±2	7±2	1.0±0.2	$\frac{31}{2}^+$	$\frac{27}{2}^+$
	279.1	2.5±0.7			$\frac{31}{2}^+$	$\frac{29}{2}^+$
3448.6	601.9	8±1			$(\frac{35}{2}^+)$	$\frac{31}{2}^+$
4103.6	655.0	0.8±0.3			$(\frac{39}{2}^+)$	$(\frac{35}{2}^+)$
4812.6	709.0	0.5±0.3			$(\frac{43}{2}^+)$	$(\frac{39}{2}^+)$
			Band 4, $\alpha = +\frac{1}{2}$			
981.2	479.3	6±1		1.0 ± 0.1	$\frac{13}{2}^+$	$\frac{15}{2}^+$
	612.1	20±2			$\frac{13}{2}^+$	$\frac{13}{2}^+$
	721.8	51±5		0.6 ± 0.1	$\frac{13}{2}^+$	$\frac{11}{2}^+$
1266.2	284.9	22±3			$\frac{17}{2}^+$	$\frac{13}{2}^+$
	152.1	47±5	0.46±0.07	0.34±0.02	$\frac{17}{2}^+$	$\frac{15}{2}^+$
	764.5	9±2			$\frac{17}{2}^+$	$\frac{15}{2}^+$
1626.5	360.3	36±4		1.1±0.1	$\frac{21}{2}^+$	$\frac{17}{2}^+$
	189.6	28±3	1.3±0.2	0.33±0.03	$\frac{21}{2}^+$	$\frac{19}{2}^+$
	800.2	9±2			$\frac{21}{2}^+$	$\frac{19}{2}^+$
2060.2	433.7	26±3		0.9±0.1	$\frac{25}{2}^+$	$\frac{21}{2}^+$
	224.9	8±1	3.2±0.6	0.34±0.03	$\frac{25}{2}^+$	$\frac{23}{2}^+$
	825.6	15±2			$\frac{25}{2}^+$	$\frac{23}{2}^+$
2566.8	506.6	19±2	5.1±0.2	1.0±0.2	$\frac{29}{2}^+$	$\frac{25}{2}^+$
	260.1	3.8±0.6			$\frac{29}{2}^+$	$\frac{27}{2}^+$
3142.4	575.6	8±2	7±3		$(\frac{33}{2}^+)$	$\frac{29}{2}^+$
	297.1	1.2±0.4			$(\frac{33}{2}^+)$	$\frac{31}{2}^+$
3778.8	636.4	1.9±0.6			$(\frac{37}{2}^+)$	$(\frac{33}{2}^+)$
4467.9	(689) [f]	<0.5			$(\frac{41}{2}^+)$	$(\frac{37}{2}^+)$
			Band 5, $\alpha = -\frac{1}{2}$			
1614.7	754.2	16±2		0.63±0.06	$\frac{19}{2}(+)$	$\frac{17}{2}^-$
1986.4	371.7	9±2		0.8±0.1	$\frac{23}{2}(+)$	$\frac{19}{2}(+)$
	691.6	24±3		0.49±0.04	$\frac{23}{2}(+)$	$\frac{21}{2}^-$
2428.8	442.4	13±2		1.04±0.04	$\frac{27}{2}(+)$	$\frac{23}{2}(+)$
	620.9	15±2		0.55±0.05	$\frac{27}{2}(+)$	$\frac{25}{2}^-$
2944.8	516.1	16±2		1.3±0.2	$\frac{31}{2}(+)$	$\frac{27}{2}(+)$
	551.7	5±1			$\frac{31}{2}(+)$	$\frac{29}{2}^-$
3538.5	593.7	4±1			$(\frac{35}{2}^+)$	$\frac{31}{2}(+)$

TABLE II. (*Continued*).

E_x (keV) [a]	E_γ (keV) [b]	I_γ^{rel} [c]	λ [d]	DCO	I_i^π [e]	I_f^π [e]
			Band 6, $\alpha = +\frac{1}{2}$			
1517.7	684.1	7±2		0.7±0.1	$\frac{17}{2}(+)$	$\frac{15}{2}-$
	869.1	5±2			$\frac{17}{2}(+)$	$\frac{17}{2}+$
1885.4	367.7	7±1		1.0±0.2	$\frac{21}{2}(+)$	$\frac{17}{2}(+)$
	621.2	6±2			$\frac{21}{2}(+)$	$\frac{19}{2}-$
2319.2	433.9	14±3			$(\frac{25}{2}+)$	$\frac{21}{2}(+)$
	544.4	6±1			$(\frac{25}{2}+)$	$\frac{23}{2}-$
2821.3	502.1	11±2			$(\frac{29}{2}+)$	$(\frac{25}{2}+)$
	461.0	<0.5			$(\frac{29}{2}+)$	$\frac{27}{2}-$
3390.3	569.0	6±1			$(\frac{33}{2}+)$	$(\frac{29}{2}+)$
			Band 7, $\alpha=+\frac{1}{2}$			
1665.2	839.1	12±2			$(\frac{21}{2}+)$	$\frac{19}{2}+$
2087.0	422.0	7±1		0.8±0.1	$(\frac{25}{2}+)$	$(\frac{21}{2}+)$
	853.0	8±2		0.67±0.02	$(\frac{25}{2}+)$	$\frac{23}{2}+$
2596.0	509.0	6±2		0.8±0.1	$(\frac{29}{2}+)$	$(\frac{25}{2}+)$
			Band 8, $\alpha = -\frac{1}{2}$			
1656.8	651.7	11±2		1.0±0.1	$(\frac{19}{2}+)$	$\frac{21}{2}+$
	830.2	12±2			$(\frac{19}{2}+)$	$\frac{19}{2}+$
2070.0	413.2	7±2			$(\frac{23}{2}+)$	$(\frac{19}{2}+)$
	634.0	8±2			$(\frac{23}{2}+)$	$\frac{25}{2}+$
	835.2	6±2		0.9±0.2	$(\frac{23}{2}+)$	$\frac{23}{2}+$
2579.0	508.4	9±2			$(\frac{27}{2}+)$	$(\frac{23}{2}+)$
	639.8	4.8±0.9		1.0±0.3	$(\frac{27}{2}+)$	$\frac{29}{2}+$
			Unassigned transitions			
1773.7	768.5	5±1		0.8±0.3	$\frac{23}{2}(+)$	$\frac{21}{2}+$
2334.7	898.4	9±1		0.9±0.2	$\frac{27}{2}(+)$	$\frac{25}{2}+$
2359.2	922.9	1.5±0.3			$(\frac{27}{2}+)$	$\frac{25}{2}+$

[a]Level energies; bandhead excitation energies have been taken from previous work [19].
[b]Accurate to 0.2 keV for most transitions. For weak or contaminated transitions, accurate to 0.5 keV.
[c]Relative γ-ray intensities [$I_\gamma(356.6)\equiv 500$] measured predominantly in the 35 MeV data set. Intensity information for γ rays at higher excitation has been supplemented with the 40 MeV data set.
[d]Branching ratio $\lambda = I_\gamma(I\rightarrow I-2)/I_\gamma(I\rightarrow I-1)$ measured from spectra corresponding to gates above spin I.
[e]Spin and parity assignments are based on the previous work [19] and on the assumption that the character of the new transitions within bands continues being stretched $E2$ in nature.
[f]Accurate to within 1 keV.

for odd-neutron nuclei. The quasiparticle vacuum is $|\phi\rangle$, which has number parity even and α_m ($\alpha_m^\dagger$) is the quasiparticle annihilation (creation) operator for this vacuum. In the calculation, we have allowed active particles from three major shells: i.e., $N = 4$, 5, and 6 ($N = 3$, 4, and 5) for neutrons (protons) as the configuration space. This is a shell model space far beyond that which a spherical shell model can handle.

The following Hamiltonian [4]:

$$\hat{H}=\hat{H}_0-\frac{1}{2}\chi\sum_\mu \hat{Q}_\mu^\dagger\hat{Q}_\mu-G_M\hat{P}^\dagger\hat{P}-G_Q\sum_\mu \hat{P}_\mu^\dagger\hat{P}_\mu \quad (3)$$

has been used. The interaction strengths are determined as follows: the quadrupole interaction strength χ is adjusted so that the known quadrupole deformation ε_2 from the Hartree-Fock-Bogoliubov self-consistent procedure [24] is obtained. It turns out that for ^{171}Yb $\varepsilon_2 = 0.265$. The monopole pairing strength G_M is adjusted to the known energy gap $G_M = \{20.12\mp 13.13[(N-Z)/A]\}A^{-1}$, with the minus (plus) sign for neutrons (protons). The quadrupole pairing strength G_Q is assumed to be proportional to G_M and the proportional constant is fixed to be 0.18 in the present work. These strengths are consistent with those used in previous works [4].

The weights f_κ in Eq. (1) are determined by diagonalizing the Hamiltonian $\hat{H}$ in the basis given by Eq. (2). This will lead to the eigenvalue equation (for a given spin I)

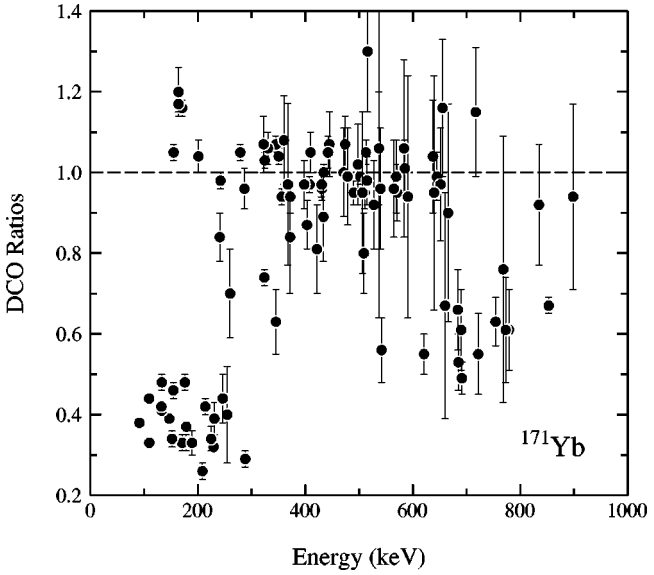

FIG. 6. DCO ratios as a function of γ-ray energy for transitions in ^{171}Yb.

$$\sum_{\kappa'} (H_{\kappa\kappa'} - EN_{\kappa\kappa'}) f_{\kappa'} = 0. \tag{4}$$

Following the basic philosophy of shell model that the same Hamiltonian should describe all the nuclear states in a given nucleus, all the theoretical bands discussed in this paper will be obtained by one single diagonalization. There is no room for individually adjusting parameters for certain states.

We would like to emphasize that solving the eigenvalue equation (4) is a process of mixing states with the same and different K's by the residual interactions. Therefore, our final states do not (and should not) have K as a good quantum number in a strict sense. Nevertheless, when the level density is not very high and the mixing is not very strong, as it is in the case of the low spin and near yrast region, a final state is usually dominated by one intrinsic K state. In this situation, we can keep using those intrinsic quantum numbers to label the final state.

Finally, we comment on the possibility of describing the other collective modes within the framework of PSM. As discussed above, the projected basis is constructed from a fixed set of quasiparticle states of BCS condensate. In this sense, the PSM is an angular momentum projected Tamm-Dancoff approximation. In principle, all the collective modes, for example, β- and γ-vibration bands, could show up from the calculation if the projected basis is sufficiently large in which all the possible configurations are mixed. In practice, however, calculations are usually done in a small size of basis (typical dimension 50) [4]. Therefore, such vibrational modes cannot be as easily obtained within PSM as in a theory with ground state correlations, such as the random phase approximation [25].

IV. DISCUSSION OF ^{170}Yb

The kinematic moments of inertia for the bands in ^{170}Yb have been plotted as a function of the square of the rotational frequency in Fig. 9, with the bands grouped according to parity. The bands have been grouped in this manner in order

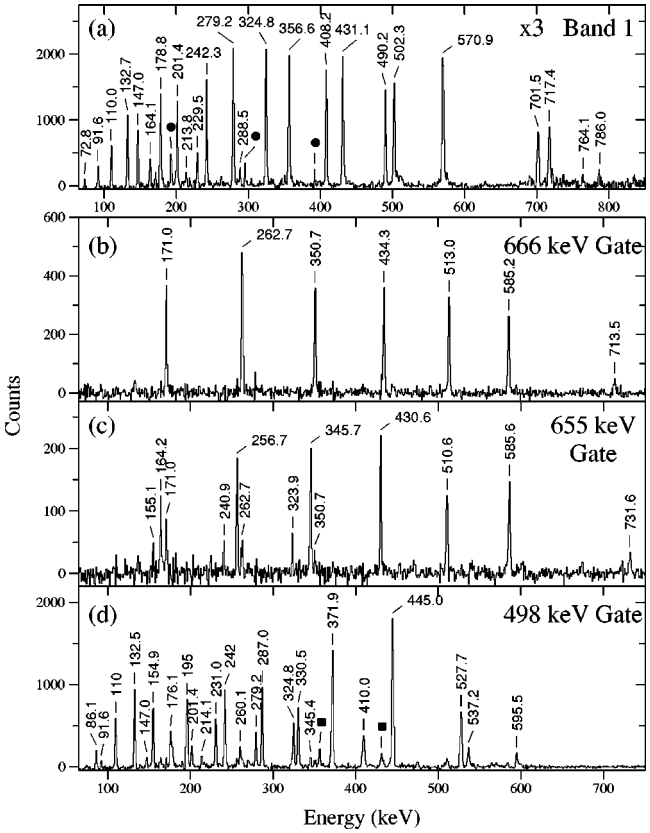

FIG. 7. Coincidence spectra for bands 1, 2, and 3 in ^{171}Yb. Band 1 is shown in panel (a) by a sum of coincidence gates set around the 637 and 645 keV transitions from the 40 MeV data set. This spectrum has been multiplied by a factor of 3 above 690 keV. The ● marks intense transitions from the bottom of the ^{170}Yb yrast band. Panels (b) and (c) show band 2 with gates on the 666 and 655 keV transitions for the $\alpha = +\frac{1}{2}$ and $\alpha = -\frac{1}{2}$ signatures, respectively. A sample spectrum from band 3 is shown in panel (d) with a gate on the 498 keV transition. The transitions marked with a box are contaminants from band 1. Panels (b), (c), and (d) are from the 35 MeV data set.

to highlight differences between the positive and negative parity bands. For example, the negative parity bands all have a flat or downward trajectory at low rotational frequencies, but the positive parity bands tend to have a sharp upward trajectory at low rotational frequency $(\hbar\omega)^2 \approx 0.05$ MeV^2. This is one factor that supports our negative parity assignment for band 10. This type of comparison shows that band 11 also has similar behavior to the other negative parity states, giving us confidence in its parity assignment. Further discussion of band assignments is continued below.

A. Band assignments

A detailed discussion of the two-quasiparticle (2QP) configurations based upon two-quasiparticle-plus-rotor calculations for the bands in ^{170}Yb can be found in the paper by Walker *et al.* [13]. Some further discussion of quasiparticle configurations was made by Goel and Jain [26], again using the two-quasiparticle-plus-rotor model, in a comparison of calculated and experimentally observed bandhead energies. Goel and Jain examined the couplings between the $i_{13/2}$ and $h_{9/2}$ neutrons, of which only two combinations have been

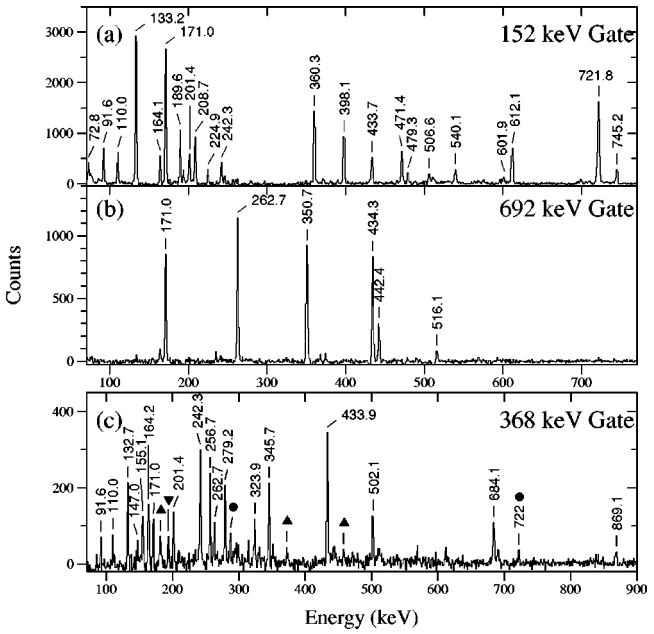

FIG. 8. Coincidence spectra for bands 4, 5, and 6 in ^{171}Yb. Panel (a) is a gate on the 152 keV γ ray showing band 4. Band 5 is shown in panel (b) by a gate on the 692 keV transition. A sample spectrum for band 6 is shown in panel (c) with a gate on the 368 keV in-band transition. Contaminant transitions from ^{170}Yb, ^{171}Yb, and ^{172}Yb are marked with filled ∇,$\bigcirc$, and $\triangle$, respectively. All the spectra shown here are from the 35 MeV data set.

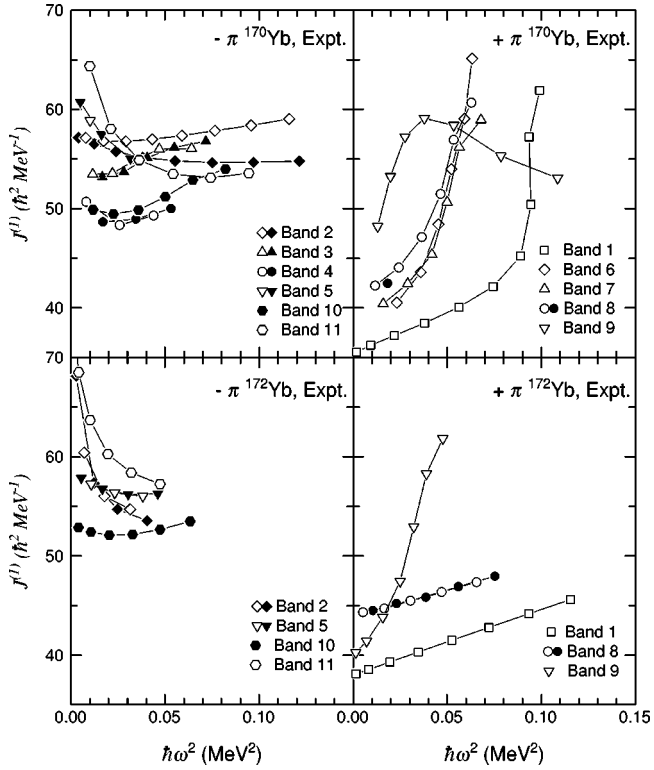

FIG. 9. Experimental values of the kinematic moments of inertia for bands in ^{170}Yb and ^{172}Yb are plotted as a function of the square of the rotational frequency.

observed experimentally, namely, $[633]\frac{7}{2}\otimes[521]\frac{1}{2}$ yielding $K^{\pi}=3^{-},4^{-}$. We compare the alignments of the 2QP bands in the even-even nucleus ^{170}Yb, to the sum of the single qp alignments found in the neighboring odd particle nuclei [27] in our configuration assignments. For the odd-particle nuclei, ^{171}Yb was used for single quasineutron states and ^{169}Tm [28] was used for single quasiproton states. A list of the observed alignment for the bands in ^{170}Yb and comparison using additivity with their suggested quasiparticle configurations can be found in Table III and is discussed below. In addition to using the comparisons of alignments in the configuration assignments, transition strength ratios have been used when applicable.

Band 1. This is the ground-state band in ^{170}Yb.

Band 2. The two previous publications [13,26] suggest a parallel coupling between the $\nu([633]\frac{7}{2}\otimes[521]\frac{1}{2})$ Nilsson states ($K=4$) for band 2 based upon two-quasiparticle-plus-rotor calculations. Support for this configuration lies in the fact that the signature splitting at higher frequencies is similar to that seen in $[633]\frac{7}{2}$ band in ^{171}Yb (see section on ^{171}Yb). Other evidence in support of this configuration is the lack of the $(\nu i_{13/2})^2$ quasiparticle alignment at $\hbar\omega=0.3$ MeV since this is blocked. We also see agreement between the theoretical and experimental transition strength ratios using the proposed configuration as discussed in Sec. VI B. Taking ^{172}Yb for comparison [29], where band 2 was also assigned the configuration $\nu([633]\frac{7}{2}\otimes[521]\frac{1}{2})$, we see from the kinematic moment of inertia plots (Fig. 9) that these bands (band 2) in both nuclei act in a similar manner.

Band 3. This band is suggested as an antiparallel coupling between the $\nu([633]\frac{7}{2}\otimes[521]\frac{1}{2})$ Nilsson states ($K=3$) in which the experimental data and two-quasiparticle-plus-rotor-model calculation bandhead energies differ by 6.6 keV [26]. Walker *et al.* [13] propose the same assignment. The alignments of the suggested $\nu([633]\frac{7}{2}\otimes[521]\frac{1}{2})$ band 3 are given in Table III. The agreement here between the observed band 3 and suggested single quasiparticle configurations is still satisfactory. In addition, the lack of a $(\nu i_{13/2})^2$ band crossing in the kinematic moment of inertia (Fig. 9) plot gives additional support to this configuration, since the $\nu i_{13/2}$ orbital is again blocked. As in the case of band 2, we also see agreement between the calculated transition strength ratio and the experimental data as discussed in Sec. VI B.

Band 4. Band 4 is proposed [13] as being based on the $\pi([523]\frac{7}{2}\otimes[404]\frac{7}{2})$ Nilsson states. This configuration seems quite reasonable within our framework of comparison as seen in Table III. Again, theoretical transition strength ratios can be used to aid in confirming the configuration assignment (see Sec. VI B).

Band 5. This weakly populated band has been previously assigned [13] the configuration of $\nu([633]\frac{7}{2}\otimes[512]\frac{5}{2})$. Our comparison of alignments shows this configuration to be reasonable. In addition, this band behaves very similarly to the $\nu([633]\frac{7}{2}\otimes[512]\frac{5}{2})$ configuration in ^{172}Yb (see Fig. 9).

Bands 6 and 7. These bands have been investigated via Coulomb excitation and attributed to the γ-vibrational mode as discussed by Riedinger *et al.* [14]. Their small alignments, as listed in Table III, at low spins are consistent with this assignment.

These bands are very similar in nature to band 8. We suggest that at higher frequencies, as usually happens, the

TABLE III. Alignment in two-quasiparticle bands for ^{170}Yb from experiment and using additivity from neighboring odd mass nuclei.

Band	K^π	Configuration [a]	Additivity $i_x(\hbar)$ [b]	^{170}Yb expt. $i_x(\hbar)$ [b]
2	4^-	$\nu([633]\frac{7}{2}\otimes[521]\frac{1}{2})$	2.94	2.02
3	3^-	$\nu([633]\frac{7}{2}\otimes[521]\frac{1}{2})$	2.08	1.73 [c]
4	7^-	$\pi([523]\frac{7}{2}\otimes[404]\frac{7}{2})$	1.32	1.35
5	6^-	$\nu([633]\frac{7}{2}\otimes[512]\frac{5}{2})$	2.43	2.20
6	2^+	γ-vib+ $\nu([512]\frac{5}{2}\otimes[521]\frac{1}{2})$	0.36	0.24 [c]
7	2^+	γ-vib+ $\nu([512\frac{5}{2}]\otimes[521]\frac{1}{2})$	0.36	0.24 [c]
8	$(3)^+$	$\nu([512]\frac{5}{2}\otimes[521]\frac{1}{2})$	1.23	0.58
9	0^+	β-vib + S-band	4.06	0.83
10	$(1)^-$	Oct vib+ $\nu([633]\frac{7}{2}\otimes[523]\frac{5}{2})$	3.66	1.37 [c]
11	$(1)^-$	Oct vib+ $\nu([633\frac{7}{2}]\otimes[523]\frac{5}{2})$	2.96	2.78

[a] ν Nilsson states taken from ^{171}Yb, $\mathcal{J}_0=36.9\ \hbar^2\ \mathrm{MeV}^{-1}$, $\mathcal{J}_1=69\ \hbar^4\ \mathrm{MeV}^{-3}$; π Nilsson states taken from ^{169}Tm, $\mathcal{J}_0=35.9\ \hbar^2\ \mathrm{MeV}^{-1}$, $\mathcal{J}_1=70\ \hbar^4\ \mathrm{MeV}^{-3}$.
[b] $\hbar\omega=0.10$ MeV.
[c] Alignment extrapolated back to $\hbar\omega=0.10$ MeV.
[d] Unable to extrapolate alignment back to $\hbar\omega=0.10$ MeV.

character of the vibrational band becomes mixed with 2QP states. Based on the similarities to band 8 shown in the moment of inertia plot, we suggest the rotational band at higher frequencies involves a coupling of the $\nu([512]\frac{5}{2}\otimes[521]\frac{1}{2})$ Nilsson states. The early back bending (see Fig. 9) of these two bands may then be attributed to the alignment of the first pair of $i_{13/2}$ neutrons. The lower frequency of this alignment in bands 6 and 7 as compared with the ground-state band, see Fig. 9, may then be understood in terms of the reduction in the pairing gap due to the blocking effect [30] caused by the sizable 2QP character of the bands for $\hbar\omega\geq 0.2$ MeV.

Band 8. This band has been previously assigned positive parity without a K value assignment [13]. Its decay characteristics imply (Fig. 2) $K\leq 4$. Inspection of ^{172}Yb reveals a $K^\pi=3^+$ rotational band built upon a mixture of the $\nu([512]\frac{5}{2}\otimes[521]\frac{1}{2})$ and $\pi([411]\frac{1}{2}\otimes[404]\frac{7}{2})$ Nilsson states [13]. Band 8 is possibly the analogous $K^\pi=3^+$ state in ^{170}Yb. This seems reasonable from comparing the kinematic moment of inertia plots of ^{170}Yb and ^{172}Yb (Fig. 9). In this figure, band 8 has very small initial moment of inertia in both nuclei as well as similar structure, with respect to the ground-state band in each nucleus. The similarities in the structure of these two bands in addition to the comparisons of moments of inertia lead us to assign a configuration of $\nu([512]\frac{5}{2}\otimes[521]\frac{1}{2})$ to this band. Bands 6, 7, and 8 in ^{170}Yb, are therefore expected to behave in a similar manner and this is indeed the case, as seen in Fig. 9. The early strong alignment at $\hbar\omega^2\approx 0.053\ \mathrm{MeV}^2$ for band 8 can thus be explained using the same blocking arguments put forth for bands 6 and 7.

Band 9. In Fig. 9, this band displays a sharp rise in moment of inertia (or alignment) at low rotational frequency. This alignment increase can be understood as a change in the character of the band from vibrational to 2QP in nature. The $K=0$ β-vibrational band is known to lie at ≈ 1 MeV in the even-even $A=166-172$ Yb nuclei and, thus, may constitute the dominant character of band 9 at low spin. The alignment gain shows the gradual mixing with the low-spin members of the neutron $(i_{13/2})^2$ band, as proposed by Walker *et al.* [13]. Very similar behavior is observed in ^{172}Yb, as shown in Fig. 9.

Bands 10 and 11. The previous assignment of $K=1$ [13] to band 11, in addition to the measured $B(E3)$ ($\approx$ 4 s.p.u.) of the 3^- state [31], suggests that this is an octupole vibration based on the ground-state band (band 1). Furthermore, a measurement of the alignment, as evidenced by the moment of inertia plot Fig. 9, shows very constant and flat alignment for band 11, $\approx 3\hbar$ higher than the ground-state band. Band 10 is suggested to be based on the unfavored octupole vibrational state. The energies and parities of the levels in this band have been firmly assigned through its interactions with bands 1 and 3. With these assignments, bands 10 and 11 show large splitting which is common between the favored and unfavored octupole-vibrational bands. This same behavior of octupole bands is shown in a plot of the moment of inertia for ^{172}Yb, Fig. 9 bands 10 and 11.

V. DISCUSSION OF ^{171}Yb

A. Configuration assignments and theoretical comparisons

A plot of the excitation energy minus a rigid-rotor reference is shown in Fig. 10 for the experimental data. The aligned angular momentum (experiment and theory) has been plotted as a function of rotational frequency for the bands in ^{171}Yb using reference Harris parameters $\mathcal{J}_0=35.8\ \hbar^2\ \mathrm{MeV}^{-1}$ and $\mathcal{J}_1=70\ \hbar^4\ \mathrm{MeV}^{-3}$ in Fig. 11. These Harris parameters were chosen following the ground-state band reference prescription of Bengtsson and Frauendorf [27,32]. Configuration assignments for the bands in ^{171}Yb are summarized below.

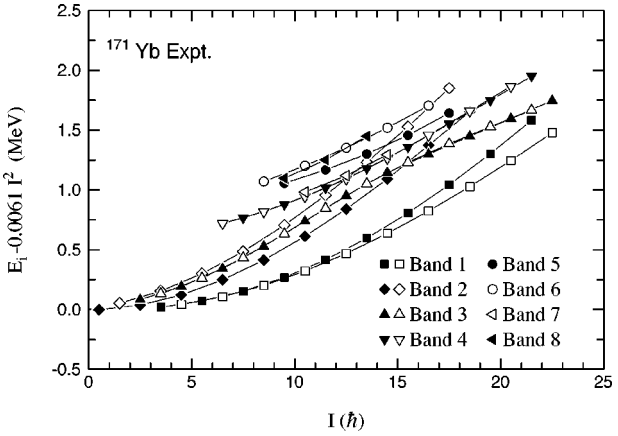

FIG. 10. Excitation energy (E_i) minus a rigid-rotor reference as a function of angular momentum for the observed bands in ^{171}Yb. The open and filled symbols differentiate between signatures of the same Nilsson configuration.

Band 1. This has been previously assigned as the $[633]\frac{7}{2}$ band [19].

Band 2. This has been previously assigned as the $[521]\frac{1}{2}^-$ band [19].

Band 3. This has been previously assigned as the $[512]\frac{5}{2}^-$ band [19].

Band 4. This band has been previously given a tentative assignment of $[505]\frac{11}{2}$ [19]. We suggest a 3QP configuration, as discussed in Sec. B.

Bands 5 and 6. Our suggestion is that these new states are associated with octupole-vibrational states built upon the $[521]\frac{1}{2}$ orbital (band 2). This assignment would be consistent with: (i) the strong high-energy dipole transitions (most likely $E1$'s) which connect bands 5 and 6 to band 2, (ii) the alignment of bands 5 and 6 which is $\approx 2-2.5\hbar$ higher than that of band 2, (iii) the large signature splitting of bands 5 and 6 which is similar to that seen in band 2, and (iv) the fact that low-lying octupole bands are observed in neighboring even-even nuclei.

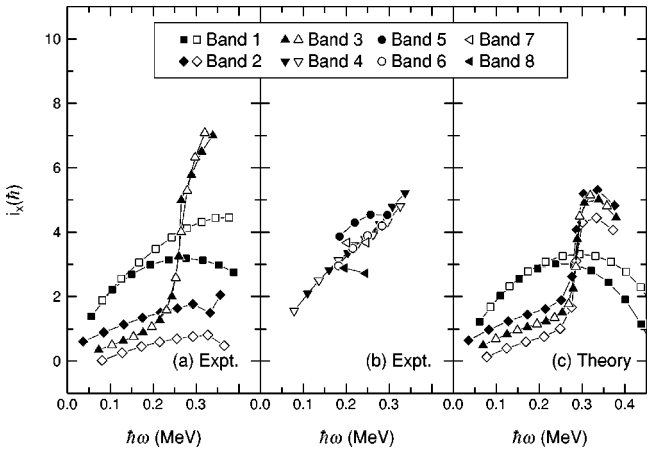

FIG. 11. Aligned angular momentum as a function of rotational frequency for (a) the observed bands 1, 2, and 3 and (b) 4, 5, 6, 7, and 8 in ^{171}Yb. Panel (c) gives the results from the PSM calculations for bands 1, 2, and 3. The open and filled symbols differentiate between signatures of the same Nilsson configuration. Harris parameters used: $\mathcal{J}_0 = 35.8\hbar^2$ MeV^{-1}, $\mathcal{J}_1 = 70\hbar^4$ MeV^{-3}.

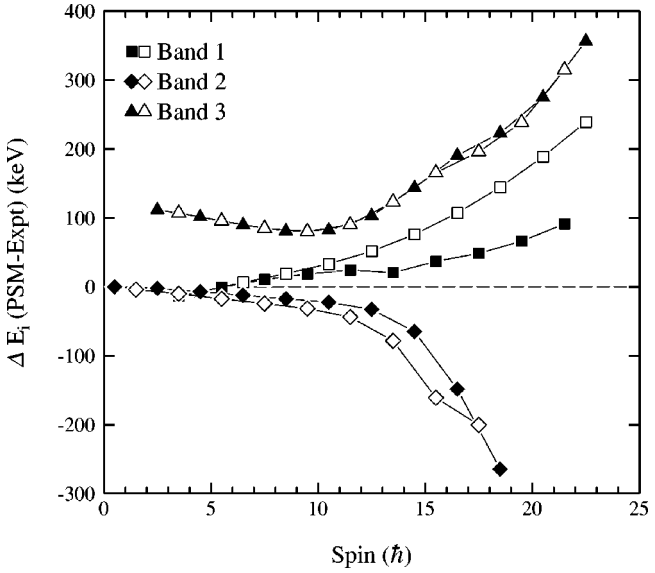

FIG. 12. Difference in excitation energy between PSM calculations and experimental data for bands in ^{171}Yb.

Bands 7 and 8. These weak structures are observed to decay to both signatures of band 1. This behavior and the fact that their alignment values are close to the alignment of band 1 (see Fig. 11), indicate the involvement of an $i_{13/2}$ neutron in their intrinsic configuration together with other components which contribute essentially zero alignment. These facts and the observation of low-lying-vibrational structures in the neighboring nuclei suggests that bands 7 and 8 are possibly β-vibrational structures based upon band 1.

PSM calculations have been made for the lowest-energy $\nu[633]\frac{7}{2}$ (band 1), $\nu[521]\frac{1}{2}$ (band 2), and $\nu[512]\frac{5}{2}$ (band 3) configurations in ^{171}Yb. Rather impressive agreement is observed between experiment and theory, particularly for bands 1 and 2. In order to enhance the differences between the experimental data and theoretical calculations, a plot of the difference in experimental and theoretical excitation energy is shown in Fig. 12. From these plots, it can be seen that band 3 is calculated to have a slightly higher energy than is shown in the experimental data. At higher spins, bands 2 and 3 are very close together in the PSM where experiment shows them moving away from one another. However, one should remember at $I = 20\hbar$ we are discussing differences of ≈ 200 keV in excitation energies of over ~ 4 MeV.

At low rotational frequencies ($\hbar\omega < 0.2$ MeV) excellent agreement in the alignment from experiment and theory is observed. However, at high rotational frequencies ($\hbar\omega > 0.25$ MeV), the agreement is not quite as good. The only band in the experimental data that goes through an obvious particle alignment is band 3 at $\hbar\omega \approx 0.25$ MeV. In the PSM calculations, the $[521]\frac{1}{2}$ and $[512]\frac{5}{2}$ bands (bands 2 and 3) are shown to back bend at $\hbar\omega \approx 0.3$ MeV. The PSM thus predicts a band crossing frequency that is slightly too high in rotational frequency for band 3 and too small a gain in aligned angular momentum.

B. Band interactions and perturbations

Interactions can occur between states of the same parity and signature, and we have used the observation of such

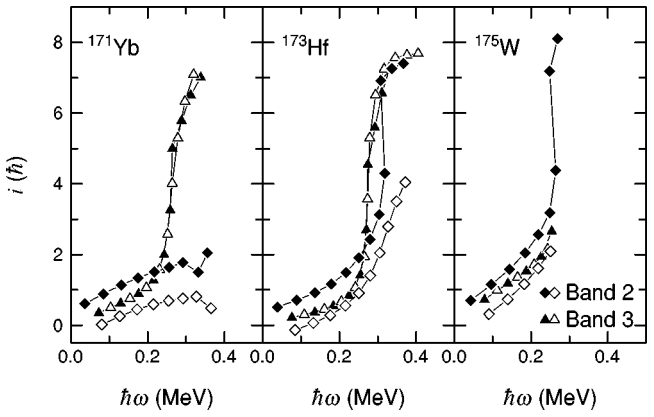

FIG. 13. Alignment plot for band 2 ($[521]\frac{1}{2}$) and band 3 ($[512]\frac{5}{2}$) in ^{171}Yb ($\mathcal{J}_0=35.8\hbar^2$ MeV^{-1}, $\mathcal{J}_1=70\hbar^4$ MeV^{-3}), ^{173}Hf ($\mathcal{J}_0=35\hbar^2$ MeV^{-1}, $\mathcal{J}_1=80\hbar^4$ MeV^{-3}) [20], and ^{175}W ($\mathcal{J}_0=28\hbar^2$ MeV^{-1}, $\mathcal{J}_1=120\hbar^4$ MeV^{-3}) [34].

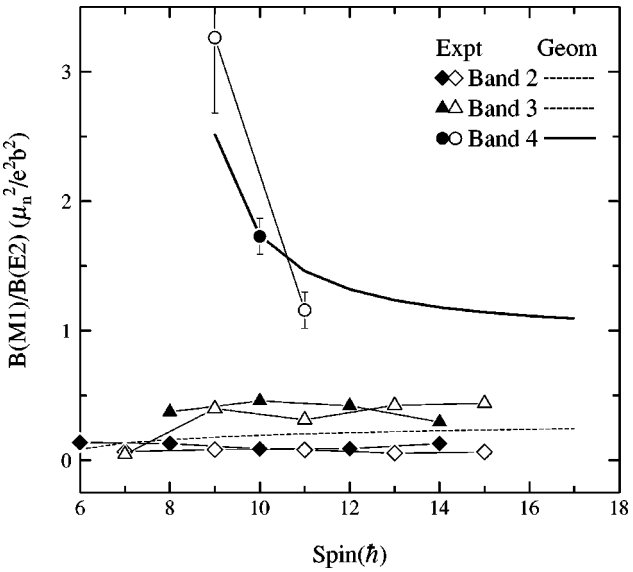

FIG. 14. Comparison of experimental and theoretical transition strength ratios (using the geometrical model [36]) for bands 2, 3, and 4 in ^{170}Yb.

perturbations in our experimental data to assist in the band assignments. In ^{171}Yb bands 2 and 3 interact at spin $I=\frac{33}{2}$ with crossover transitions between both bands being observed. The interaction between bands shows up as a perturbation in the excitation energy and the alignment (Figs. 10 and 11). The excitation energy of the $\alpha=+\frac{1}{2}$ signatures of bands 2 and 3 cross at $I=15.5\hbar$. Above this point, band 3 is pushed down a little in excitation energy. This results in a slight increase in the alignment of band 3, which can be seen as the separation of signatures of band 3 in the alignment plot at $\hbar\omega\approx0.26$ MeV. A simple two level mixing calculation for bands 2 and 3 at $I=\frac{33}{2}$ gives an interaction matrix element of 25 keV. An interaction at the same spin for the same configurations is also seen in ^{173}Hf [20] with an interaction matrix element of 17 keV. A comprehensive study of other similar perturbations found in rare-earth nuclei has been compiled by Hagemann *et al.* [33].

Band 4 has been previously suggested tentatively [19] to have a configuration of $[505]\frac{11}{2}^-$. This negative parity assignment allows the possibility of interactions with bands 2 and 3. In the excitation energy plot (Fig. 10), band 4 is shown to come within 7 keV of band 2 at $I=\frac{37}{2}$. The lack of any perturbation indicates that band 4 is more likely to be of positive parity. We suggest a 3QP configuration of $\nu[[633]\frac{7}{2}\otimes[512]\frac{5}{2}\otimes[521]\frac{1}{2})$ which translates into $\nu[$(band 1 $\alpha=+\frac{1}{2}$) $\otimes$ (band 2 $\alpha=+\frac{1}{2}$) $\otimes$ (band 3 $\alpha=\pm\frac{1}{2}$)]. Additional support for this assignment comes from blocking arguments and the transition strength measurements and calculations discussed below.

TABLE IV. Parameters for theoretical $B(M1)/B(E2)$ values for ^{170}Yb.

Band	Q_0	g_R	g_1	K_1	i_1	g_2	K_2	i_2
2	7.6	0.41	−0.20	3.5	2.2	−0.23	0.5	1.0
3	7.6	0.41	−0.20	3.5	2.2	−0.23	0.5	1.0
4	7.6	0.41	0.80	3.5	0.21	1.26	3.5	1.1

VI. FIRST $\nu i_{13/2}$ BAND CROSSING AND TRANSITION STRENGTH RATIOS IN ^{170}Yb AND ^{171}Yb

A. The first $\nu i_{13/2}$ band crossing

The first back bend in this region of nuclei is due to the alignment of a pair of $i_{13/2}$ neutrons between $\hbar\omega=0.25$ and 0.3 MeV. An alignment plot is shown in Figs. 11(a) and 11(b) for the observed bands in ^{171}Yb. Figure 11(c) shows the predictions of the PSM calculations. Since band 1 is the $[633]\frac{7}{2}$ band, this first $i_{13/2}$ alignment is blocked. This blocking argument also applies to band 4 where no back bend is observed (see Fig. 11), since we suggest that this band has a configuration involving the $i_{13/2}$ neutron orbital. Band 3 back bends as expected at about $\omega\approx0.25$ MeV. Band 2, however, shows no signs of back bending, a result in contrast to the expectations of the PSM. This anomaly may result from the interaction of bands 2 and 3 in the back bending region together with the fact that in the other $N=101$ isotones there is a slight delay in the band crossing frequency of the $[521]\frac{1}{2}$ band with respect to the $[512]\frac{5}{2}$ (see Fig. 13). However, the delays in the $N=101$ isotones seem to be much smaller than the delay found in ^{171}Yb. Further experimental work to observe band 2 to higher spin is necessary to resolve this question.

B. Transition strength ratios

Transition strength ratios $[B(M1{:}I\rightarrow I-1)/B(E2{:}I\rightarrow I-2)]$ give clear indications about the quasiparticle content of a rotational band and can thus aid in band identification. Experimental measurements of the ratios of reduced transition probabilities for ^{170}Yb and ^{171}Yb will be compared with a semiclassical [35] version of Dönau's geometrical model [36], as described in Ref. [10], as well as with PSM predictions. In the experimental measurements, the $E2/M1$ mixing ratio (δ) is assumed to be small and therefore negligible.

1. $B(M1{:}I\rightarrow I-1)/B(E2{:}I\rightarrow I-2)$ values in ^{170}Yb

Experimental transition strength ratios have been measured for bands 2, 3, and 4 (the strongly coupled bands) in

TABLE V. Parameters for theoretical $B(M1)/B(E2)$ values for ^{171}Yb.

Band	No.	Q_0	g_R	g_1	K_1	i_1	g_2	K_2	i_2	g_3	K_3	i_3
$\nu[633]_{\frac{7}{2}}$	1	7.7	0.41	−0.18	3.5	2.2						
$\nu[521]_{\frac{1}{2}}$	2	7.7	0.41	−0.23	0.5	0.1						
$\nu[512]_{\frac{5}{2}}$	3	7.7	0.41	−0.24	2.5	0.48						
3QP band	4	7.7	0.41	−0.18	3.5	2.2	−0.24	2.5	0.24	−0.23	0.5	0.35

^{170}Yb. The intrinsic electric quadrupole moment for ^{170}Yb has been tabulated by Raman [37] as $Q_0 = 7.6\ e$ b. The core g factor g_R is taken as $g_R = Z/A = 0.41$. The K values and g factors used in the theoretical calculations have been assigned in accordance with the band assignments discussed earlier. Using these band assignments, the single-particle alignments have been taken from the measured alignments of the neighboring single particle nuclei ^{169}Tm (bands 2 and 3) and ^{171}Yb (band 4). These theoretical parameters are shown in Table IV.

A graph of both experimental and theoretical transition strength ratios for bands 2, 3, and 4 of ^{170}Yb are plotted in Fig. 14 as a function of spin. Bands 2 and 3 are both based upon the $[633]_{\frac{7}{2}}$ and $[521]_{\frac{1}{2}}$ orbitals. Following the geometrical model as discussed in Ref. [10] we thus expect these two bands to have the same calculated transition strength ratios. As shown in Fig. 14, the calculated $B(M1)/B(E2)$ ratios lie between band 2 and band 3 giving good agreement between experiment and the geometrical theory. For band 4 it is only possible to extract the transition strength ratios for three states without introducing large errors ($>25\%$). Using the parameters in Table IV which correspond to the configuration assigned to this band in Sec. IV A, we find that the theory agrees with the experimental value as shown in Fig. 14.

2. $B(M1{:}I\rightarrow I-1)/B(E2{:}I\rightarrow I-2)$ values in ^{171}Yb

Transition strength ratios for bands 1, 2, 3, and 4 in ^{171}Yb have been measured experimentally and are compared with the theoretical PSM calculations as well as Dönau's geometrical model [36]. The value of Q_0 was determined by averaging the quadrupole moments from the neighboring even-even nuclei ^{170}Yb and ^{172}Yb as tabulated by Raman [37]. As in ^{170}Yb, the value for $g_R = Z/A = 0.41$ was taken. The values for g_j, where $j = l + \frac{1}{2}$, were taken from Frauendorf [38]. The g_j value for $j = l - \frac{1}{2}$ (i.e., the $[521]_{\frac{1}{2}}$ band) was calculated using the magnetic moment found in Ref. [39]. These parameters are listed in Table V. The results for the theoretical calculations of $B(M1)/B(E2)$ are shown in Fig. 15 along with the experimentally measured values.

In Fig. 15 the signature splitting of band 1 can be seen in the experimental data as a distinct separation between the filled and unfilled symbols. The PSM calculation is close to the measured data and even has a comparable amount of signature splitting as the experimental data at higher spins. Only the unfavored signature is shown for band 2, since there are no dipole transitions from the favored to the unfavored signature. The agreement between the theory and experiment is reasonable for band 3. Using the 3QP configuration for band 4 results in theoretical transition strength ratios that are reasonably close at low spin but which deviate at high spin. We attribute this difference to a lowering of the effective K value of the experimental band with increasing spin, as the band mixes with the other close lying 3QP bands. A small and reasonable reduction of $2\hbar$ in the effective K value would bring the theoretical curve for band 4 shown in Fig. 15 to about 0.33 at high spins in close agreement with experimental observations.

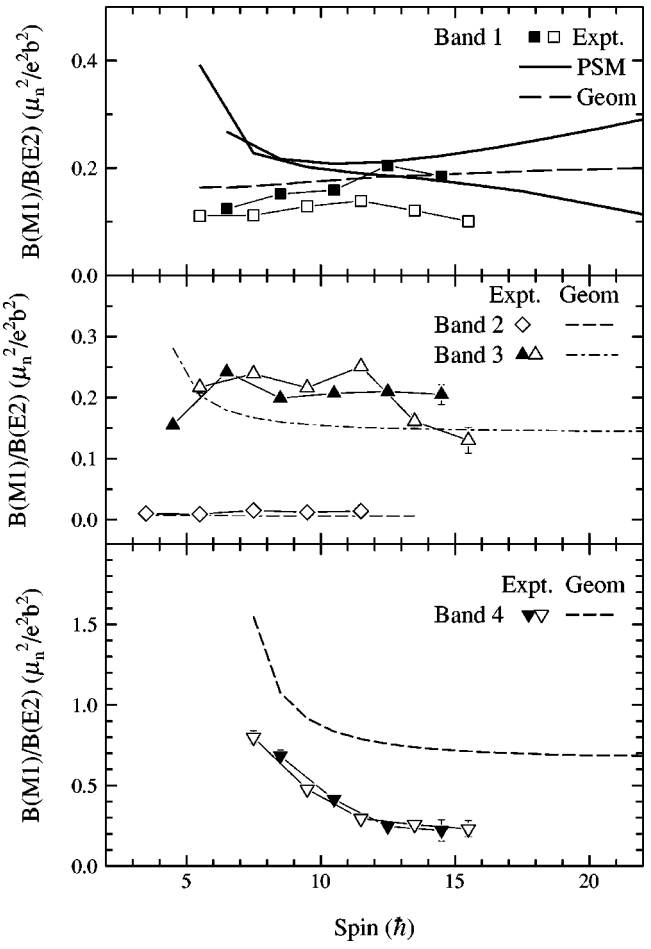

FIG. 15. Transition strength ratios for the bands in ^{171}Yb. The experimental data points are indicated with symbols and connected by solid lines and the theory is given by the lines indicated. The top panel shows the experimental ratios for the $[633]_{\frac{7}{2}}$ band (band 1) along with the projected shell model and geometrical model calculations. The PSM calculations have been made including the signature splitting term. The middle panel shows experimental data of the $B(M1)/B(E2)$ ratios for the $[521]_{\frac{1}{2}}$ and $[512]_{\frac{5}{2}}$ bands (bands 2 and 3) along with the geometrical model calculation. Similarly, the bottom panel shows the 3QP band 4 with the geometrical model estimate.

VII. CONCLUSION

The reaction ^{170}Er(α,4n) at 40 MeV was used to produce high-spin states of ^{170}Yb and allowed an assignment of 67 new γ transitions and one new rotational structure to this nucleus. The structures in ^{170}Yb have been described in terms of both quasiparticle and vibrational excitations.

High-spin states of ^{171}Yb were produced using the ^{170}Er(α,3n) reaction at 35 MeV. This experiment allowed 110 new γ rays and 4 new rotational band structures to be added to the level scheme of ^{171}Yb. The present study represents the first detailed investigation of excited states in an odd-N nucleus by the projected shell model.

Overall the PSM calculations show a most impressive agreement with experiment for ^{171}Yb, demonstrating the power of this model for describing low- to medium-spin rotational structures in deformed rare-earth nuclei. The PSM is not able to describe all the experimental observations, however, with differences still remaining for certain configurations in the back bending region.

ACKNOWLEDGMENTS

Special thanks to D. C. Radford, W. T. Milner, and H. Q. Jin for their wonderful software support. Thanks also to F. K. McGowan, N. R. Johnson, and R. Darlington for their marvelous help with the targets. We would also like to thank Dr. J. X. Saladin for his crucial role in creating the Pitt-FSU γ-ray array and to the UK Gamma-Ray Community for the loan of several HPGe detectors. This work was supported by the U.S. National Science Foundation and the State of Florida. This research was performed under the auspices of the U.S. Department of Energy for Lawrence Livermore National Laboratory under Contract No. W-7405-ENG-48. M.A.R. and J.S. acknowledge the receipt of a NATO Collaborative Research Grant.

[1] *Table of Isotopes*, edited by R.B. Firestone and V.S. Shirley (Wiley, New York, 1996).
[2] I.Y. Lee, S.J. Asztalos, M.-A. Deleplanque, B. Cederwall, R.M. Diamond, P. Fallon, A.O. Macchiavelli, L. Phair, F.S. Stephens, G.J. Wozniak, S. Frauendorf, J.A. Becker, E.A. Henry, P.F. Hua, D.G. Sarantites, and C.H. Yu, Phys. Rev. C **56**, 753 (1997).
[3] S.L. Tabor, M.A. Riley, J. Döring, P.D. Cottle, R. Books, T. Glasmacher, J.W. Holcomb, J. Hutchins, G.D. Johns, T.D. Johnson, T. Petters, O. Tekyi-Mensah, P.C. Womble, L. Wright, and J.X. Saladin, Nucl. Instrum. Methods Phys. Res. B **79**, 821 (1993).
[4] K. Hara and Y. Sun, Int. J. Mod. Phys. E **4**, 637 (1995).
[5] K. Hara and S. Iwasaki, Nucl. Phys. **A348**, 200 (1980); **A430**, 175 (1984).
[6] K. Hara and Y. Sun, Nucl. Phys. **A529**, 445 (1991); **A531**, 221 (1991); **A537**, 77 (1992).
[7] Y. Sun and J.L. Egido, Nucl. Phys. **A580**, 1 (1994).
[8] Y. Sun and J.L. Egido, Phys. Rev. C **50**, 1893 (1994).
[9] Y. Sun, D.H. Feng, and S. Wen, Phys. Rev. C **50**, 2351 (1994).
[10] D.E. Archer, M.A. Riley, T.B. Brown, J. Döring, D.J. Hartley, G.D. Johns, T.D. Johnson, R.A. Kaye, J. Pfohl, S.L. Tabor, J. Simpson, and Y. Sun, Phys. Rev. C **52**, 1326 (1995).
[11] S.X. Wen, H. Zheng, S.-G. Li, G.-S. Li, G.-J. Yuan, P.-F. Hua, P.-K. Weng, L.-K. Zhang, P.-S. Yu, C.-X. Yang, H.-B. Sun, Y.-B. Liu, Y.-Z. Liu, Y. Sun, and D.H. Feng, Phys. Rev. C **54**, 1015 (1996).
[12] D.C. Radford, Nucl. Instrum. Methods Phys. Res. A **361**, 297 (1995).
[13] P.M. Walker, W.H. Bentley, S.R. Faber, R.M. Ronningen, R.B. Firestone, F.M. Bernthal, J. Borggreen, J. Pedersen, and G. Sletten, Nucl. Phys. **A365**, 61 (1981).
[14] L.L. Riedinger, E.G. Funk, J.W. Mihelich, G.S. Schilling, A.E. Rainis, and R.N. Oehlberg, Phys. Rev. C **20**, 2170 (1979).
[15] D. Barneoud, J. Boutet, J. Gizon, and J. Valentin, Nucl. Phys. **A138**, 33 (1969).
[16] P. Sen and H. Bakhru, Z. Phys. A **281**, 263 (1977).
[17] B.S. Dzhelepov and S.A. Shestopalvoa, Bull. Russ. Acad. Sci. Phys. **56**, 1650 (1992).
[18] D.G. Burke, B. Zeidman, B. Elbek, B. Herskind, and M. Olsen, Mat. Fys. Medd. K. Dan. Vidensk. Selsk. **35**, 2 (1966).
[19] Th. Lindblad, H. Ryde, and D. Barneoud, Nucl. Phys. **A193**, 155 (1972).
[20] B. Fabricius, G.D. Dracoulis, T. Kibédi, A.E. Stuchbery, and A.M. Baxter, Nucl. Phys. **A523**, 426 (1991).
[21] C.G. Andersson, G. Hellström, G. Leander, I. Ragnarsson, S. Åberg, J. Krumlinde, S.G. Nilsson, and Z. Szymański, Nucl. Phys. **A309**, 141 (1978).
[22] Y. Sun, S. Wen, and D. H. Feng, Phys. Rev. Lett. **72**, 3483 (1994).
[23] P. Ring and P. Schuck, *The Nuclear Many Body Problem* (Springer-Verlag, Berlin, 1980).
[24] I.-L. Lamm, Nucl. Phys. **A125**, 504 (1969).
[25] J.L. Egido, H.J. Mang, and P. Ring, Nucl. Phys. **A339**, 390 (1980).
[26] A. Goel and A.K. Jain, Phys. Lett. B **337**, 240 (1994).
[27] R. Bengtsson, S. Frauendorf, and F.-R. May, At. Data Nucl. Data Tables **35**, 15 (1986).
[28] D. Barnéoud, C. Foin, S. André, H. Abou-Leila, and S.A. Hjorth, Nucl. Phys. **A230**, 445 (1974).
[29] P.M. Walker, S.R. Faber, W.H. Bentley, R.M. Ronningen, and R.B. Firestone, Nucl. Phys. **A343**, 45 (1980).
[30] J.D. Garrett, O. Andersen, J.J. Gaardhøje, G.B. Hagemann, B. Herskind, J. Kownacki, J.C. Lisle, L.L. Riedinger, W. Walus, N. Roy, S. Jonsson, H. Ryde, M. Guttormsen, and P.O. Tjøm, Phys. Rev. Lett. **47**, 75 (1981).
[31] D.G. Burke and B. Elbek, Mat. Fys. Medd. K. Dan. Vidensk. Selsk. **36**, No. 6 (1967).
[32] R. Bengtsson and S. Frauendorf, Nucl. Phys. **A327**, 139 (1979).
[33] G.B. Hagemann, H. Ryde, P. Bosetti, A. Brockstedt, H. Carlsson, L.P. Ekström, A. Nordlund, R.A. Bark, B. Herskind, S. Leoni, A. Bracco, F. Camera, S. Frattini, M. Mattiuzzi, B. Million, C. Rossi-Alvarez, G. de Angelis, D. Bazzacco, S. Lunardi, and M. De Poli, Nucl. Phys. **A618**, 199 (1997).
[34] P.M. Walker, G.D. Dracoulis, A. Johnston, J.R. Leigh, M.G. Slocombe, and I.F. Wright, J. Phys. G **4**, 1655 (1978).
[35] V.P. Janzen, Z.-M. Liu, M.P. Carpenter, L.H. Courtney, H.-Q.

Jin, A.J. Larabee, L.L. Riedinger, J.K. Johansson, D.G. Popescu, J.C. Waddington, S. Monaro, S. Pilotte, and F. Dönau, Phys. Rev. C **45**, 613 (1992).
[36] F. Dönau, Nucl. Phys. **A471**, 469 (1987).
[37] S. Raman, C.H. Malarkey, W.T. Milner, C.W. Nestor Jr., and P.H. Stelson, At. Data Nucl. Data Tables **36**, 1 (1987).
[38] S. Frauendorf, Phys. Lett. **100B**, 219 (1981).
[39] P. Raghavan, At. Data Nucl. Data Tables **42**, 189 (1989).